

# AN EVALUATION OF THE DURABILITY OF POLYMER CONCRETE BONDS TO ALUMINUM BRIDGE DECKS

Huiying Zhang

Thesis submitted to the Faculty of the  
Virginia Polytechnic Institute and State University  
in partial fulfillment of the requirements for the degree of

MASTER OF SCIENCE  
IN  
ENGINEERING MECHANICS

APPROVED:

David A. Dillard, Chairman

John G. Dillard

Richard E. Weyers

April 30, 1999

Blacksburg, Virginia

**Keywords:** Durability, Polymer concrete overlays, Strain energy release rate,  
Mixed-mode fracture test, Epoxy, Aluminum, Adhesive bond

©1999, Huiying Zhang

# AN EVALUATION OF THE DURABILITY OF POLYMER CONCRETE BONDS TO ALUMINUM BRIDGE DECKS

Huiying Zhang

## ABSTRACT

The objective of this study is to evaluate the bond durability of an epoxy-based polymer concrete wearing surface bonded to aluminum bridge decks. In the bridge design, an aluminum alloy bridge deck is used with a polymer concrete wearing surface. A modified mixed mode flexure fracture test was developed to assess the bond durability of specimens aged in the following environmental conditionings: 30°C [86°F], 98% RH; 45°C [113°F], 98% RH; 60°C [140°F], 98% RH; freezing and thawing; salt ( $N_aCl$ ) water soak; and 60°C [140°F], dry. The exposure times varied from none to twelve months. The critical strain energy release rate ( $G_c$ ) of the bond was determined using a compliance technique. In spite of considerable scatter in the data, the results suggested that the interfacial bond toughness had been degraded by exposure conditions. The aging appeared to affect the polymer concrete overlay (silica aggregates/epoxy bond) as well. Fracture analysis and finite element modeling were completed for linear elastic behavior. Analytical and numerical solutions were in reasonably good agreement. Characterization of the bridge components and failure specimens were accomplished using analytical measurements including thermal gravimetric analysis (TGA), differential scanning calorimetry (DSC), and dynamic mechanical analysis (DMA). Techniques employed in the surface analysis included x-ray photoelectron spectroscopy (XPS) and scanning electron microscopy (SEM).

## ACKNOWLEDGEMENTS

I would like to thank Dr. David A. Dillard for his patient guidance and advice during the course of my studies at Virginia Tech. Thanks are also due to Dr. John G. Dillard and Dr. Richard E. Weyers for serving on my advisory committee. Additionally, I would like to thank David Mokarem for helping with specimens conditioning and fracture tests, electrical engineer Bob Simonds for his help on running some tests, Frank Cromer for his help on running SEM and XPS, and Raul Andruet for teaching me to use ABAQUS. Most of all, I would like to thank my parents for their constant encouragement and support during my education. Finally, I show my special appreciation to Buo Chen, Didier R. Lefebvre and all the other folks working in the Adhesion Mechanics Lab for their help and advice on my research.

# Contents

<b>1</b>	<b>Introduction</b>	<b>1</b>
1.1	Background . . . . .	1
1.2	Research Objectives . . . . .	3
1.3	Overview of the Study . . . . .	3
<b>2</b>	<b>Test Method Development</b>	<b>4</b>
2.1	Abstract . . . . .	4
2.2	Introduction . . . . .	4
2.3	Test Method Development . . . . .	7
2.4	Analytical Evaluation . . . . .	10
2.5	Finite Element Analysis . . . . .	11
2.6	Conclusions . . . . .	12
<b>3</b>	<b>Experiments</b>	<b>22</b>
3.1	Abstract . . . . .	22
3.2	Introduction . . . . .	22
3.3	Experiments . . . . .	25
3.3.1	Material system and specimen geometry . . . . .	25
3.3.2	Specimen postcuring . . . . .	25
3.3.3	Specimen conditioning . . . . .	26
3.3.4	The auxiliary adherend bonding . . . . .	27
3.3.5	Testing . . . . .	27

3.4	Results and Discussion . . . . .	28
3.5	Post-failure Surface Analysis . . . . .	30
3.5.1	Scanning electron microscopy (SEM) . . . . .	30
3.5.2	X-ray photoelectron spectroscopy (XPS) . . . . .	31
3.6	Summary and Conclusions . . . . .	32
<b>4</b>	<b>Material Characterization</b>	<b>45</b>
4.1	Introduction . . . . .	45
4.2	Polymer Concrete . . . . .	45
4.2.1	Shear modulus . . . . .	45
4.2.2	Stress-strain testing . . . . .	48
4.2.3	Stress relaxation testing . . . . .	50
4.3	Properties of Neat Polymer . . . . .	50
4.3.1	Thermal gravimetric analysis (TGA) . . . . .	50
4.3.2	Differential scanning calorimetry analysis (DSC) . . . . .	50
4.3.3	Dynamic mechanical analysis (DMA) . . . . .	51
4.3.4	Thermal mechanical analysis (TMA) . . . . .	51
4.3.5	Solvent absorption . . . . .	52
4.3.6	Stress-strain testing . . . . .	53
4.4	Properties of the Aluminum . . . . .	54
4.4.1	Strain-stress testing . . . . .	54
4.4.2	Thermal mechanical analyzer (TMA) . . . . .	54
<b>5</b>	<b>Improving Bonds to Cured Epoxy</b>	<b>72</b>
5.1	Introduction . . . . .	72
5.2	Static DCB Testing . . . . .	73
5.2.1	Introduction . . . . .	73
5.2.2	Testing and analytical solution . . . . .	73
5.2.3	Testing results and analysis . . . . .	74

<b>6</b>	<b>Conclusions</b>	<b>83</b>
<b>A</b>	<b>ABAQUS Input File - Sandwich Specimen</b>	<b>91</b>

# List of Figures

2.1	NCA type specimen (original specimen geometry) . . . . .	14
2.2	Dimensions of a typical sandwich specimen . . . . .	15
2.3	Specimen geometries for fracture tests: (a) Three-point bend (b) Four-point bend (c) Standard MMF test (d) Modified MMF test . . . . .	16
2.4	Schematic of the modified mixed-mode flexure test configuration used for testing each end of the notched specimens . . . . .	17
2.5	Transformed section for composite bar . . . . .	18
2.6	Finite element model of the middle part of a MMF specimen, with crack propagating along the interface . . . . .	19
2.7	The FEA mesh near the crack tip, showing two J-integral contours . . . . .	20
2.8	Comparison of the strain energy release rate calculated using analytical solution and FEA, for P=2500 N . . . . .	21
3.1	Aluminum bridge deck beam . . . . .	33
3.2	Three-point bending used to initiate the debond at the primary (upper) interface	34
3.3	Data fit for typical compliance method (Data from the specimens with the same aging condition and aging time) . . . . .	35
3.4	Plot of typical MMF loading-unloading curve . . . . .	36
3.5	Critical energy release rate for control and aged specimens, showing numerical averages and error bars with $\pm\sigma_{n-1}$ . . . . .	37
3.6	Comparison of G (for controls) from compliance method, FEA, analytical equation, showing numerical averages and error bars with $\pm\sigma_{n-1}$ . . . . .	38

3.7	Failed aluminum surface . . . . .	39
3.8	Failed polymer concrete surface . . . . .	40
3.9	XPS survey spectrum of failed polymer concrete surface . . . . .	41
3.10	XPS survey spectrum of failed aluminum surface . . . . .	42
4.1	Geometry of the three-point bending test . . . . .	55
4.2	The three-point bending test results . . . . .	56
4.3	Comparison of the measured elastic modulus with predictions based on three models . . . . .	57
4.4	Comparison of the measured ratio with predictions based on three models . . . . .	58
4.5	Geometry of the tensile test specimen . . . . .	59
4.6	Relaxation test results for a sandwich sample at room temperature . . . . .	60
4.7	Relaxation test results for a sandwich sample at -33°C . . . . .	61
4.8	TGA data for Flexolith 216R . . . . .	62
4.9	DSC data for Flexolith 216R (2nd run) . . . . .	63
4.10	DMA data for Flexolith 216R . . . . .	64
4.11	CTE data for Flexolith 216R . . . . .	65
4.12	Water mass uptake curves for Flexolith 216R under different conditions . . . . .	66
4.13	Different solvent mass uptake curves for Flexolith 216R . . . . .	67
4.14	CTE data for aluminum . . . . .	68
5.1	Schematic of a filled joint . . . . .	76
5.2	Three types of DCB specimens . . . . .	77
5.3	Schematic of symmetric DCB, pure mode I . . . . .	78
5.4	Load and unload curve for DCB testing . . . . .	79
5.5	Photograph of the failure surface of a DCB specimen without DMAC . . . . .	80
5.6	Photograph of the failure surface of a DCB specimen with DMAC . . . . .	81

# List of Tables

3.1	Environmental conditioning matrix . . . . .	43
3.2	XPS element analysis of different surfaces . . . . .	44
4.1	Tensile test results of PC . . . . .	69
4.2	Tensile test results of neat polymer . . . . .	70
4.3	The properties of Al alloy 6063-T6 . . . . .	71
5.1	DCB test results for G . . . . .	82

# Chapter 1

## Introduction

### 1.1 Background

The need for change in traditional bridges made of steel-reinforced concrete has been acknowledged since the 1960s. One major problem is the chloride ion-induced corrosion of the reinforcing steel, which accounts for much of the rehabilitation costs [1]. To date, much effort has been made to improve basic concrete properties to protect the reinforcing steel. Effective solutions for deteriorating infrastructure, however, have been elusive.

Presently, the most used rehabilitation methods for concrete decks are latex-modified concrete overlays (LMC), low slump dense concrete overlays (LSDC) and membranes with a hot-mixed asphalt wearing surface (HMAM) [1]. These methods have been developed by state Departments of Transportation and industry. The service life of these rehabilitation's is limited because chloride-contaminated concrete is left in place and corrosion continues at a slow but detectable rate under the overlay. Service lives for LMC or LSDC rehabilitation overlays and HMAM rehabilitation overlays are 22-26 years and 10-15 years, respectively [1]. The service life of such bridges, original plus rehabilitation, is much shorter than the present 75 to 100 year design life [1].

To increase the life of newly constructed bridge decks, epoxy coated reinforcing steel (ECR) was developed and promoted by the Federal Highway Administration (FHWA) as a long term corrosion protection method for steel in concrete. The reinforcing bars were coated with epoxy to prevent the chloride ions from contacting the steel. ECR is the most widely used corrosion protection system. However, recent evidence demonstrated that the service life extension has been estimated to be 5 to 10 years in Virginia [1]. The estimate is valid for the case where the coating has not debonded from the bar when the chlorides arrive at the depth of the steel. In most cases involving adequate cover depths and moderately low permeable concrete, the epoxy has debonded from the bar before chloride arrives at the steel surface [1].

In some situations, lightweight, rapidly-installed, extruded aluminum bridge deck systems may offer cost-effective replacements for deteriorated bridge decks. Recently Reynolds Metals Company has developed a structural design for bridge decks that does not focus on rehabilitation or protection of the steel-reinforced concrete system. These new bridge decks consist of extruded aluminum beams which are welded together to form deck sections. Polymer concrete overlays, similar to those used to resurface portland cement concrete bridge decks, are applied to the top surface to provide a skid-resistant and durable surface for traffic. Polymer concrete (PC) is a composite material in which aggregate is bound together with a polymer binder [2].

In Virginia, polymer concretes have been widely tested and used as protective overlays for portland cement concrete bridge beams. Epoxy polymer concrete overlays have shown desirable durability when properly installed on these surfaces, with service lives being 10-25 years dependent upon traffic conditions [3]. Our current interest is how this system may perform in contact with aluminum bridge deck surfaces. Differences in the coefficients of thermal expansion (CTE) between the PC and aluminum, and the interfacial characteristics (different surface pretreatments) may affect the performance of this material system.

## 1.2 Research Objectives

The objective of this project is to evaluate the durability performance of a Reynolds Metals Company aluminum bridge beams. Three major variables affecting the bond system during the service life of a bridge are moisture, temperature, and applied loading . The inherent differences in the materials result in thermal expansion mismatches which could result in significant stresses at the interface, especially in the vicinity of flaws, holidays, joints, and coating terminations. Moisture-induced swelling and mechanical loads due to rolling loads could also produce stresses which could, over time, lead to delamination. In order to assess the durability of these bonds, and to gain a better understanding of the interfacial region between the PC and aluminum, the present study has been initiated to investigate the properties of PC/aluminum bonds. The primary focus of the project involves a series of mixed-mode flexure (MMF) fracture tests of bonded specimens, many of which have been exposed to several different conditioning environments.

## 1.3 Overview of the Study

This thesis is divided into five chapters. Chapter 1 includes a research background, the objective of this work and the overview of the study. Chapter 2 and chapter 3 are written as technical papers dealing with the evaluation of the durability of polymer concrete bonds to aluminum bridge decks. Chapter 2 is on the topic of test method development. Chapter 3 concerns the experiments and results. Both of them contain their own abstract, introduction, analysis, summary and conclusions. I expect to submit them in a revised form for publication in Journal of Adhesion. Chapter 5 deals with the material properties measurements. Because some experimental procedures are not necessary for the technical papers, this part forms an individual chapter. The material properties will be added to the second paper (experiments part) later. Chapter 5 summarizes the major conclusions drawn from chapters 2 and 3, as well as other suggestions related to this research effort.

# Chapter 2

## Test Method Development

### 2.1 Abstract

A modified mixed-mode flexure fracture test was developed to assess the bond toughness between polymer concrete overlays and aluminum for bridge deck applications. Fracture analysis and finite element modeling were completed for linear elastic behavior. Analytical modeling and numerical solutions are in reasonably good agreement.

### 2.2 Introduction

Aluminum bridge decks coated with a polymer concrete (PC) wearing surface are a bridge design developed by Reynolds Metals Company to solve the chloride ion-induced corrosion problem in steel-reinforced concrete bridges. The focus of this paper is to develop a test method to evaluate the polymer concrete coating's performance in contact with the aluminum bridge deck's surface.

Bond strength is the ability of coating to adhere to its substrate. Bond strengths depend on the adhesion and cohesion properties of the epoxy binders, the cleanliness, texture, and moisture content of the substrate and other factors related to chemistry [2]. An evaluation of the adhesive for use should include an evaluation of not only its tensile properties, such

as strength and modulus, but also its performance and durability under real exposure conditions. Reynolds Metals Company has conducted pull-out tests to measure the strength of the PC/aluminum bond [4]. Unfortunately, the strength test can't mimic the real performance of the bridge during its service life. The pullout strength test simulated that the polymer concrete coating would delaminate from the aluminum bridge decks as a whole piece. Usually, the bond fails by initiating from holidays, coating terminations, joints, and other flaws that might be present in actual bridge decks, and then propagates along the interface. A fracture mechanics approach is based on the presence and growth of flaws, and it is very effective to predict crack presence, growth, fracture and failure in adhesive joints [5]. In this study, the fracture mechanics approach is used to evaluate the performance of the polymer concrete/Al bond. An experimental technique needs to be chosen to measure parameter - the strain energy release rate,  $G_c$ .

A number of testing methods can be used for fracture toughness determination. For example, the double cantilever beam (DCB) and end-notched flexure (ENF) tests are for materials under pure mode I (opening) and mode II (shear) conditions, respectively. DCB was introduced for fracture toughness testing by Ripling and Mostovoy [6]. This method is suitable for a sandwich specimen with a very thin adhesive layer in between. Williams [7] gave the analysis for DCB specimens, and showed that the corrected beam theory is accurate and reliable. Blackman et al [8] gave the calculation of adhesive fracture energies from DCB test specimens. Rackestraw et al [9] showed research on the rate dependence of fracture toughness of the DCB testing. Mall [10] and Blackman et al [11] used DCB to study adhesive bonds between composite adherends. Other people used DCB to test bond between metal or wood. The ENF geometry can be used to determine mode II fracture properties of adhesive bonds. Russell and Street [12] used ENF to study graphite/epoxy bonded systems.

Several mixed-mode flexure tests have been used for fracture toughness measurements. Loading methods for mix-mode fracture tests are slightly different, Russell and Street [12]

used the name of mixed-mode flexure (MMF) test first. They used three-point bend loading to do research on the composites laminates.

A single leg bending (SLB) test was used by Davidson and Sundararaman [13] to test interfacial fracture toughness of glass/epoxy and alumina/niobium bonds. They evaluated its suitability for interfacial toughness measurements, and showed that the SLB test may be used to determine the fracture toughness of most bimaterial interfaces over a reasonably large range of mode mixities. MMF and SLB are equivalent geometries, but different people named them different ways.

In the case of the four-point flexure test [14], a constant moment exists between the inner loading points. Therefore, the strain energy release rate of the interface crack exhibits steady behavior, where  $G$  is independent of the crack length. Ritter used this test method to study the crack propagation in polymer adhesive/glass sandwich specimens [14] and epoxy/PMMA bonds [15]. Charalambides et al [16] used this specimen to study Al/PMMA bonds. Klingbeil and Beuth [17] did interfacial fracture testing of deposited metal layers under four-point bending. Preliminary tests had been tried on our specimens, and the testing results showed that plastic deformation occurred in the aluminum substrate after debonding, which made the analysis very complicated.

Zhang and Shang [18] developed a flexural peel (FP) technique to study the crack behavior along a bimaterial behavior. The technique is also a mixed-mode test. Cao and Evans [19] did some experimental studies on the fracture resistance of bimaterial interfaces. The specimen geometries for interface fracture resistance measurements in their studies included symmetric double cantilever beam, asymmetric cantilever beam, four-point flexure and composite cylinder. They established mixed mode fracture conditions for a model bimaterial interface by introducing interface cracks into different specimen geometries. The interface fracture resistance increased with increase in phase angle of loading.

The notched coating adhesion (NCA) [20] test is a test method which can reduce the conditioning time by decreasing the diffusion path. Single lap joints (SLJ) and double cantilever beam (DCB) specimens with a width of 25 mm may take several months to equilibrate, depending on the temperature and adhesive [20]. For an NCA specimen with a 1 mm coating, only a couple hours is required to saturate the bond and interface region in the same condition. Chang et al [20] showed that the NCA is a effective accelerated method to estimate adhesive performance and durability for coating specimens. The specimens were loaded in tension and the test geometry resulted in interfacial debonds.

During the bridges' service life, significant shear and peel stresses may be induced at the PC/Al interface under mechanical loads, moisture swelling, and thermal loads. These stresses are especially significant around breaks in the coating and near free edges. The polymer concrete material bonding system will be subjected to opening and shear mode for crack initiation and propagation. A test method should be selected to simulate these stresses for the interfacial fracture testing of this material system. This paper presents a modified mixed-mode flexure fracture test for studying the durability of the bridge system. As will be seen, the loading method makes the crack tend to stay in the interface.

## 2.3 Test Method Development

Notched coating adhesion (NCA) specimens [20] were anticipated for measuring the fracture toughness of the interface. An initial section of the extruded beams was sliced into specimens. Notches were cut into the polymer layer with an abrasive wheel, producing the characteristic NCA geometry illustrated in figure 2.1. These notches simulate the flaws in the bridge, and they serve to focus the stresses to produce an interfacial failure in NCA type specimens.

Most NCA specimens consist of a thin layer of adhesive bonded to a single substrate. The

initial specimens had a 7 mm thick coating. Because of the massive nature of the specimens (compared with other NCA specimens), these specimens were subjected to bending rather than tensile loading. Preliminary tests conducted in 3-point and 4-point bending suggested that the NCA type specimen would be suitable. Based on these findings, a sufficient quantity of the beams were fabricated from which could be cut into specimens. Unfortunately, these subsequent beams did not meet the coating thickness specifications. The coating thickness was about half of that required. Some specimens had polymer thicknesses of only 4 mm in numerous places. This reduced thickness resulted in too little energy being stored in the coating. Sufficient energy storage capacity was needed to induce debonding of the coating. The test was altered as described below. A decision was made to bond an additional aluminum layer onto the polymer concrete surface to provide sufficient energy storage capacity to induce debonding of the coating. The surface of the auxiliary aluminum layer was then prepared to achieve adequate bonding. The aluminum beams were then bonded onto the NCA specimens to achieve satisfactory specimens for testing. To avoid impeding the diffusion of moisture into the specimens to be exposed to environmental conditioning, these auxiliary plates were not bonded in place until after the environmental conditioning had been achieved on the specimens being aged. The geometry of the sandwich specimen is shown in figure 2.2.

In preliminary 3-point and 4-point bending tests for specimens without auxiliary adherend, the adherend of Al deck specimen plastically deformed before the crack propagated. In this case, the fracture analysis could be complicated by the nonlinear behavior. Moment diagrams for four different test methods are shown in figure 2.3. For methods (a) and (b), the highest moment focuses at the notch, which could result in substrate's yielding before debonding. Both methods (c) and (d) have less moment at the notch, therefore plastic deformation in the adherend can be avoided.

During the service life of the bridge, the shear and peel stresses are induced in the

Al/epoxy interface by mechanical loads, moisture swelling and thermal loads. A mixed mode flexure (MMF) test may simulate these stresses which actually occur. As the name of the test implies, the debond at the interface is under combined opening and shear mode loading. A modified mixed-mode flexure (MMF) test is illustrated in figure 2.4. In the standard MMF test, the applied load is centered between the two supports. Because of the dimensions on the notched specimens, and the desire to increase the length available for debonding, the load was located at the quarter point as shown in modified MMF test diagram. The advantages of the method include:

1. Plastic deformation of the aluminum substrate is avoided during the test. This should simplify the analysis which would become quite complex if adherend yielding were to occur [21].
2. Each sample can be tested twice (by flipping the specimen end for end), permitting two data points per specimen.
3. Only one debond tip propagates during loading, thus simplifying the monitoring of debond growth. If three-point or four point-bending were conducted on specimens with the notch centered, two debonds would propagate simultaneously.
4. The cure of an adhered layer on a substrate may result in shrinkage and corresponding residual tensile stress, which may subsequently be altered by the test temperature and moisture induced swelling. For the case of a coating debonding from a substrate, these residual stresses become of significant importance. They are less important when a stiff adherend is bonded to the coating in the sandwich fashion used here, because the adherend reduced the energy release in the debonded layer.
5. Debonds tend to be interfacial.

In preliminary tests, the viscoelastic flow in the polymer concrete at room temperature reduced the available strain energy release rate significantly. Since it is difficult to accurately separate the two factors - viscoelastic flow and crack propagation, the MMF tests were

conducted at a temperature of  $-33^{\circ}\text{C}$  to reduce the influence of viscoelasticity. This also simulates the low temperatures experienced during winter when bond toughness may be reduced and when residual stresses are greatest. The tests could not be run in a thermal chamber since it is necessary to read the crack length during the testing. The specimens were cooled in dry ice for five hours before testing. Since the specimens had large size and mass, and one test only took about nine minutes, it is assumed that the temperature of the specimens did not change. The testing temperature was assumed to be  $-33^{\circ}\text{C}$ , the temperature of dry ice.

## 2.4 Analytical Evaluation

A linear elastic fracture mechanics solution for the MMF specimen geometry (figure 2.4) is derived analytically from beam theory. The linear elastic fracture mechanics may only be applied to those materials which obey Hooke's law [22]. The strain energy,  $U$ , stored within the composite beam is given in equation 2.1.

$$U = \int_{-L_1}^0 \frac{\frac{1}{4}P^2x^2}{2E_2I} dx + \int_0^a \frac{\frac{1}{4}P^2x^2}{2E_2I_2} dx + \int_a^{L_2} \frac{\frac{1}{4}P^2x^2}{2E_2I} dx + \int_{L_2}^L \frac{\frac{3}{4}P^2(L-x)^2}{2E_2I} dx \quad (2.1)$$

where  $P$  is the applied load,  $a$  the initial crack length,  $E$  the elastic modulus of the polymer concrete,  $E_2$  the elastic modulus of the aluminum,  $I$  the second moment of area of the sandwich beam,  $I_2$  the moment of inertia of the aluminum beam substrate ( $t_2$ ), and  $x, L_1, L_2$  and  $L$  are depicted in figure 2.4.  $I$  is the second moment of area of a equivalent transformed cross-section with an elastic modulus of the aluminum substrate. Equations 2.2 and 2.3 are given [23] for calculating the moment of inertial of the composite beam [24], as shown in figure 2.5.  $b$  is the beam width.  $n_2$ , is called the transformation factor and  $n_2 = E/E_2$ .

$$I = b \left[ \frac{1}{12}(t_2^3 + t_1^3 + n_2h^3) + t_1 \left( t_2 + h + \frac{t_1}{2} - y \right)^2 + n_2h \left( t_2 + \frac{h}{2} - y \right)^2 + t_2 \left( \frac{t_2}{2} - y \right)^2 \right] \quad (2.2)$$

$$y = \frac{2t_1(t_2 + h) + t_1^2 + 2n_2t_2h + n_2h^2 + t_2^2}{2(t_1 + n_2h + t_2)} \quad (2.3)$$

Therefore the strain energy release rate upon crack propagation becomes

$$G = -\frac{1}{b} \frac{\partial U}{\partial a} = \frac{P^2(L_1 + a)^2}{32bE_2} \left( \frac{1}{I_2} - \frac{1}{I} \right) \quad (2.4)$$

$G$  is the applied strain energy release rate.

The derivation is based on the simple beam theory, in which case the length to depth ratio should be higher than 10. Due to the shear effects in the thick adhesive layer (where the shear modulus is relative low compared to the adherend), the equation may not be valid. Further correction factors may be needed to use the equation properly according the FEA shown below.

## 2.5 Finite Element Analysis

A finite element model of the sandwich specimen was developed and analyzed using the ABAQUS<sup>1</sup> software package. The meshes consisted of 3072 eight-noded, plane stress, quadrilateral elements. Meshes of the middle part of the specimen are shown in figure 2.6. The model consisted of outer layers of aluminum alloy and an inner layer of polymer concrete. The geometry of the numerical analysis used is shown in figure 2.2 and figure 2.4. The simple supports are used in FEA. At -33°C, the aluminum alloy has an elastic modulus  $E = 68 \text{ GPa}$  (experimental results). The polymer concrete has an elastic modulus  $E = 9.2 \text{ GPa}$  and Poisson's ratio  $\nu = 0.19$  (experimental results showing in chapter 4). The crack was simulated to propagate along the primary bond between the specially prepared extrusion and the polymer concrete. Finer meshes were used near the crack tip and interface, as shown in figure 2.7. The J-integral values were calculated along the contours around the crack tip vicinity.

---

<sup>1</sup>ABAQUS is a trademark of Hibbitt, Karlsson, and Sorenson, Providence, RI.

In general cases, the J-integral value equals to G value within the linear elastic region. Figure 2.8 shows a comparison of J-integral from the FEM analysis with the strain energy release rate, G, from the analytical solution as a function of crack length at a constant load of 2500 N. The numerical analysis gave a solution which was higher than the results from analytical solution. One possible reason is that the analytical evaluation was based on a simple beam theory. The dimension of the specimens has a length to depth ratio of 7. The specimen was not perfect for simple beam theory. Due to the shear effects in the thick adhesive layer (where the shear modulus is relative low compared to the adherend), the equation may not be valid. Further correction factors may be needed to use the equation properly according the FEA. In this case, the finite element analysis should give a more accurate solution than the analytical evaluation. An ABAQUS input file is attached in Appendix A. The comparison between the FEA and experimental results will be shown in next chapter.

## 2.6 Conclusions

Based on this research work, the following conclusions have been reached:

The mixed-mode flexure fracture test method was chosen for evaluating the fracture toughness of polymer concrete bonds to aluminum bridge decks. Plastic deformation of the aluminum substrate is avoided using the modified MMF test. Each sample can be tested twice and only one debond tip propagates each time, thus simplifying the monitoring of debond growth. The cure of an adhered layer on a substrate may result in shrinkage and corresponding residual tensile stress. A sandwich fashion specimen can make the residual stresses less important.

The polymer concrete coating showed extensive time-dependence of elastic modulus at room temperature. Viscoelastic flow in the polymer concrete reduced the available strain energy release rate. The results of relaxation tests at room temperature and at -33°C showed

that decreasing the test temperature can reduce the influence of the viscoelasticity. The test technique included conditioning the specimens in dry ice for 5 hours before testing. The testing temperature was assumed to be  $-33^{\circ}\text{C}$ , the temperature of dry ice.

A finite element model was constructed for the sandwich specimen. The numerical analysis provides J-integral values, which are in reasonable agreement with G calculated from the analytical solution.

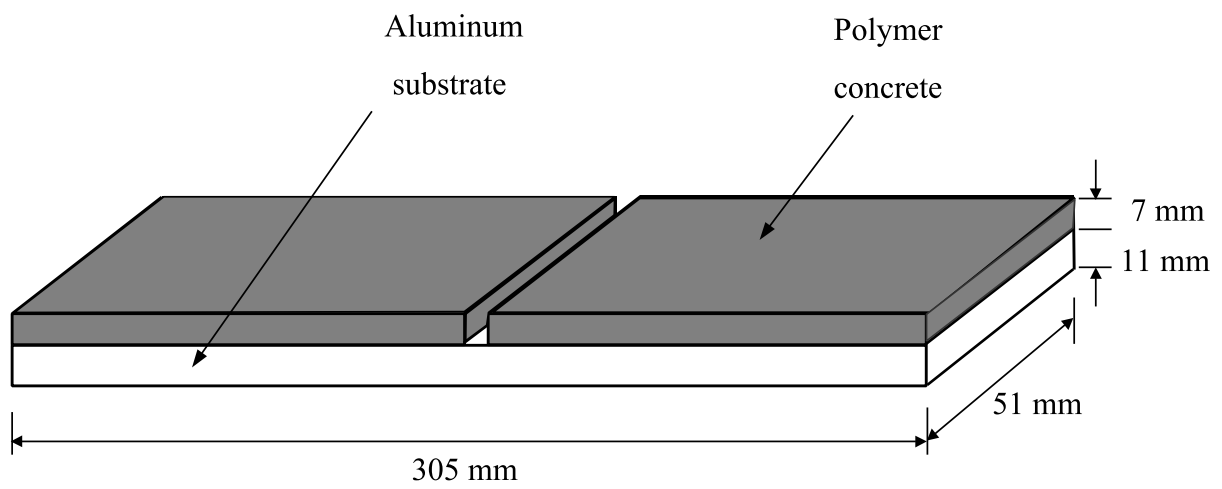


Figure 2.1: NCA type specimen (original specimen geometry)

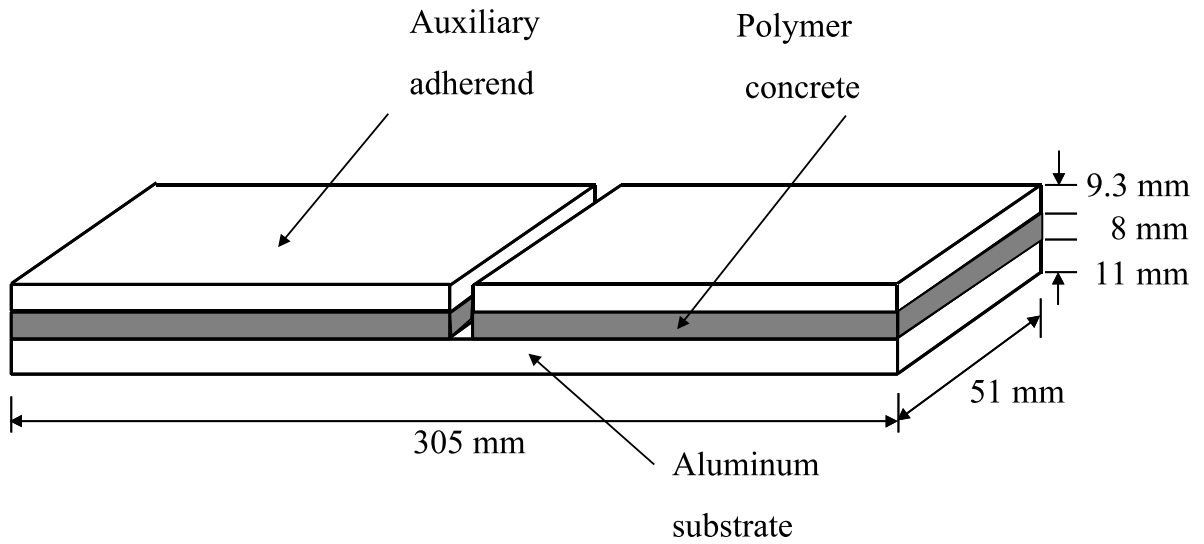


Figure 2.2: Dimensions of a typical sandwich specimen

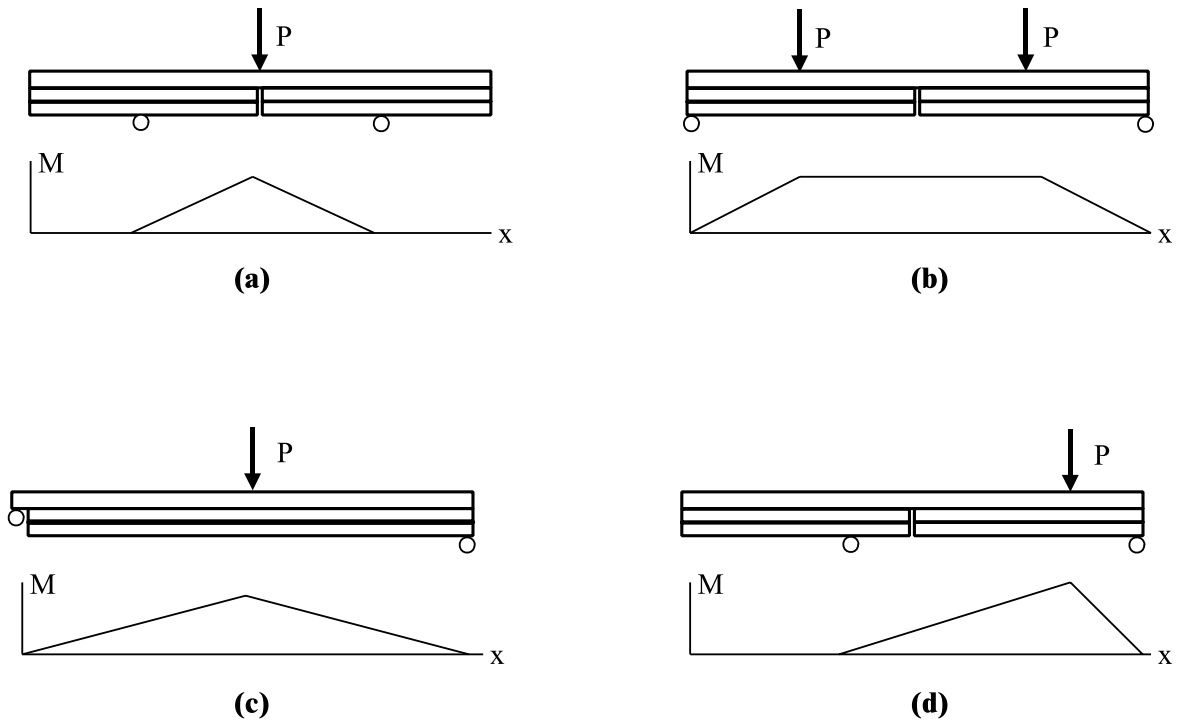


Figure 2.3: Specimen geometries for fracture tests: (a) Three-point bend (b) Four-point bend (c) Standard MMF test (d) Modified MMF test

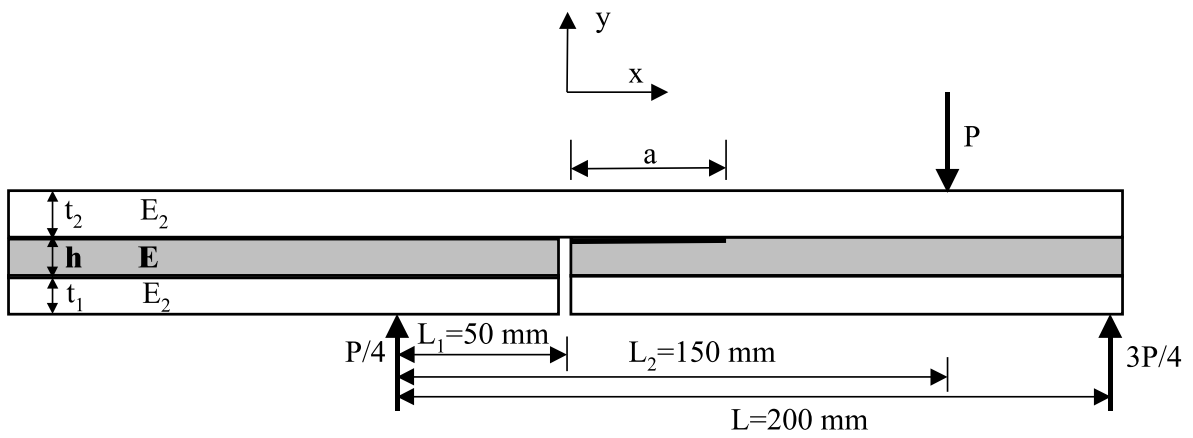


Figure 2.4: Schematic of the modified mixed-mode flexure test configuration used for testing each end of the notched specimens

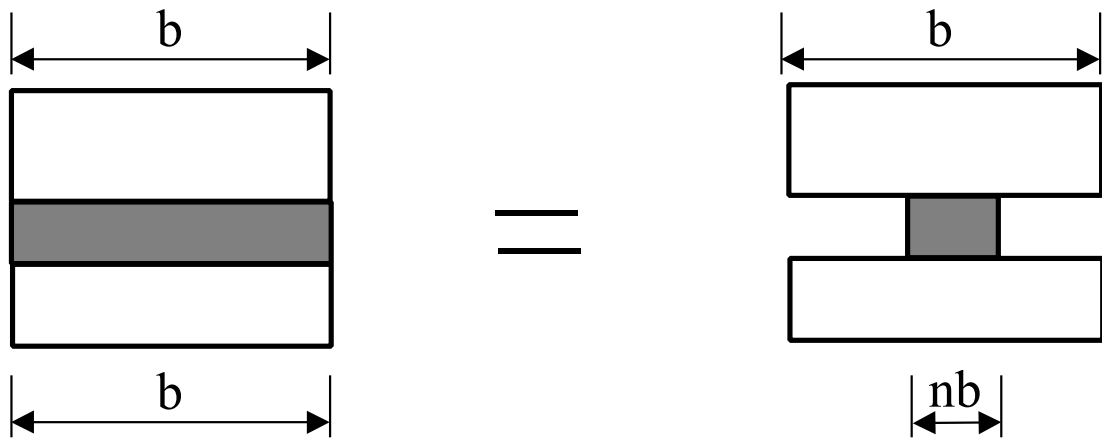


Figure 2.5: Transformed section for composite bar

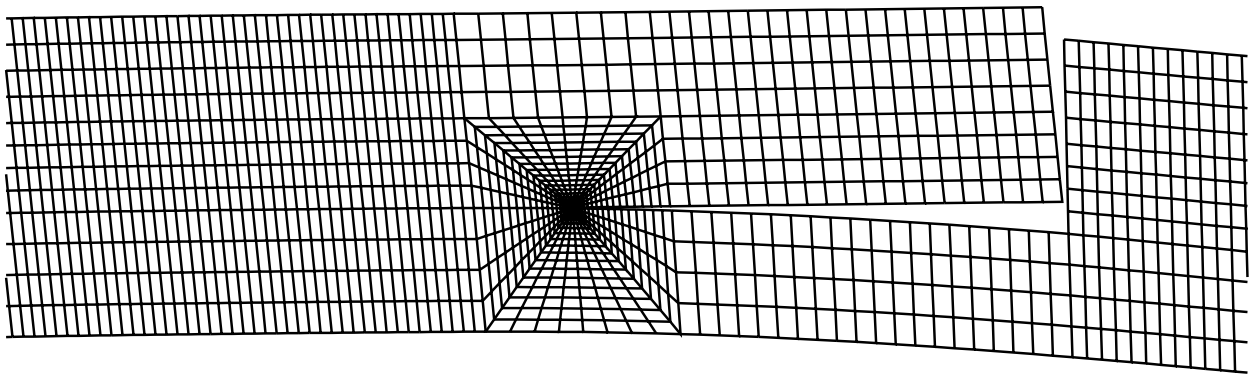


Figure 2.6: Finite element model of the middle part of a MMF specimen, with crack propagating along the interface

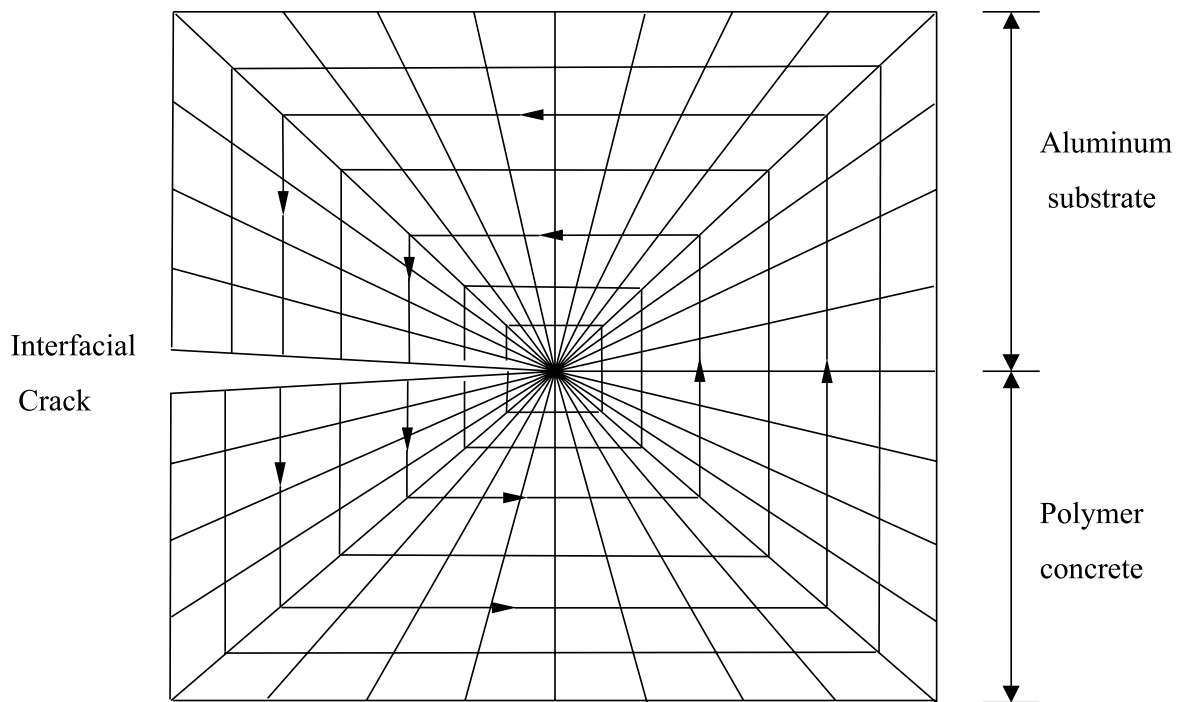


Figure 2.7: The FEA mesh near the crack tip, showing two J-integral contours

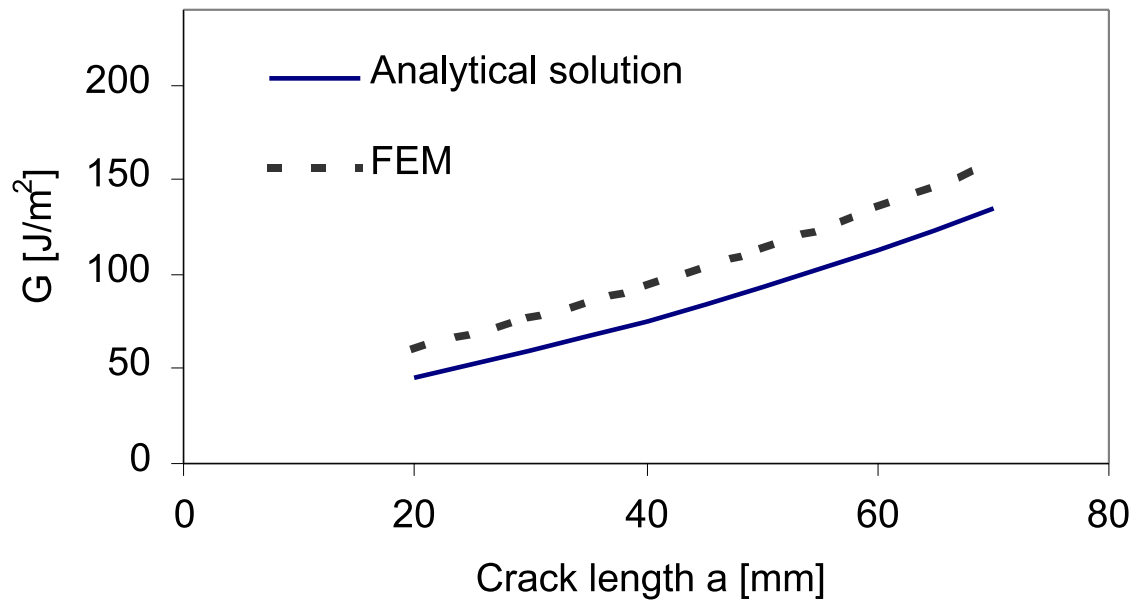


Figure 2.8: Comparison of the strain energy release rate calculated using analytical solution and FEA, for  $P=2500$  N

# Chapter 3

## Experiments

### 3.1 Abstract

This study evaluates the bond durability of an epoxy-based polymer concrete wearing surface bonded to aluminum bridge decks. A modified mixed-mode flexure fracture test was employed to assess the bond durability of the controls and specimens aged in different environmental conditions. The exposure times vary from none to twelve months. The critical strain energy release rate ( $G_c$ ) of the bond was determined using a compliance technique. The testing results suggest that the interfacial bond toughness was degraded by the exposure conditions. The aging appeared to affect the polymer concrete coating (silica aggregate /epoxy bond) as well.

### 3.2 Introduction

Environment is becoming increasingly hostile to steel-reinforced concrete due to the de-icing salts [25], acid rain, gasoline, pollution chemicals [2]. Some replacement choices for the steel-reinforced concrete are high-density concrete overlays, latex modified concrete overlays, membrane/asphalt systems, cathodic-protection systems, epoxy-coated reinforcing bars, and thin polymer concrete (PC) overlays [2]. The choices have different advantages and disadvantages. One of the attractive advantages of the polymer concrete system over other overlay

systems, is the short construction time. The shorter construction time means saving money from traffic controlling and labor costs, which makes the bridge more cost effective. Another important advantage of PC is the good chloride resistance, high impermeability and fatigue resistance. The surface pretreatment is the most important factor in achieving the proper bond and best performance. Two disadvantages of PC are that the cure rate of PC is dependent on the application temperature and moisture during cure could cause problems.

Polymer concrete used in this material system is a composite material consisting of two phases - epoxy matrix phase and silica aggregate filler phase. The epoxy has a low modulus of elasticity to withstand the stresses created by freeze-thaw cycles, moisture and traffic. The viscous deformation of the epoxy reduces stress. The high aggregate content can minimize the adverse effect of curing shrinkage, increase stiffness, strength and mechanical damping, reduce permeability to liquids, and reduce cost as well [26]. By incorporating inorganic aggregate into PC overlays, it is possible to lower the coefficient of thermal expansion of the PC. The properties of composite materials are determined by the properties of the components, by the shape of the filler, the interface between the phases [26] and other factors.

An adhesive is defined as a material to be applied to surfaces of materials. An adhesive can join the materials together and resist separation [27]. Adhesion means the attraction between an adhesive and substrate(s) [27]. The adhesive and substrate(s) are joined together to form an adhesively bond system. The system consists of an adhesive, substrate(s), appropriate surface pretreatment to the substrate(s) and the interphase/interface regions between the first three components [28]. Durability is the ability of the material system to withstand the induced stresses without debonding. A variety of factors may affect the durability of adhesive joints, such as applied mechanical loads, environments, material properties of adhesive and substrates, bonding geometry, and residual stresses in bond. Durability assessment and life prediction for adhesive joints are an important issue.

In many cases, durability testing needs to be accelerated by increasing load, humidity level, and temperature, to finish the laboratory research work in months. Bowditch [29] pointed out that elevating the temperature can accelerate degradation rates, but high temperature may facilitate a degradation mechanism that may never occur at a low temperature; therefore careful choice of an accelerated test method is necessary.

In a study of the durability of adhesive joints, Bowditch [29] investigated the effects of water on adhesive joints. He came to a conclusion that water can affect both the physical and mechanical properties of the adhesive itself and also the nature of the interface or interphase that exists between it and the substrate. Brewis [30] used single lap joints to investigate the effect of humidity on the durability of aluminum-epoxide joints. Neve and Shanahan [31] studied the effects of humidity on an epoxy adhesive. They did research on the durability of Al/adhesive and steel/adhesive bonds after various times of aging.

Parker [32] investigated the environmental durability of aluminum joints with different pretreatments. Holubka [33] studied the durability of adhesive bonds to zinc-coated steel; the focus of the paper was on the effects of corrosive environments on lap shear strength. Adams [34] was interested in the effect of temperature on the strength of adhesive joints. He showed that thermal effects lead to significant changes in the stress state of lap joints. Also the stress/strain properties of polymeric adhesive vary considerably with temperature. The combined effect of the two factors was illustrated by the variation of strength of single lap shear joints. Many other papers on the topic of evaluating the adhesive bond durability have been published ([35], [25]).

In this work, specimens have been evaluated after being aged in different environmental conditions including freezing-thawing cycling, salt (NaCl) water soak, and elevated temperature and moisture exposure. The performance of the bonds after aging has been compared. The durability was evaluated by using the MMF test on sandwich specimens.

## 3.3 Experiments

### 3.3.1 Material system and specimen geometry

Polymer concrete-coated extrusions of 6063-T6 aluminum were supplied by Reynolds Metals Company. The aluminum bridge deck beams were extruded and a proprietary Reynolds surface pretreatment was used to prepare the surfaces prior to bonding to convert the reactive aluminum oxide to a more inert species [4]. Equal volumes of Flexolith 216R<sup>1</sup> A and B components were mixed thoroughly, then silica aggregate (2.35 times the volume of the mixed Flexolith) was stirred into the epoxy. The mixture was spread over the surface of the treated aluminum beams. The coating was cured at room temperature for seven days (information provided by Reynolds Metals Co.). The thickness of the aluminum substrate is 11 mm. The thickness of the polymer concrete coating varied from 4 mm to 9.5 mm. The volume fraction of the particle filler was 70 percent (information provided by Reynolds Metals Co.). Following receipt of the extrusions, the top plates were cut from the cross-sections and then cut into 51 mm  $\times$  305 mm specimens by a commercial water-jet cutting operation. Notches were introduced into the polymer layer with an abrasive wheel, producing the characteristic NCA [20] geometry illustrated in figure 2.1. After appropriate aging times, two additional aluminum bars were bonded onto the polymer concrete surface. The geometry of the sandwich specimen is shown in figure 2.2.

### 3.3.2 Specimen postcuring

All samples were placed into an oven at 60°C for 24 hours to make sure that the adhesive was fully cured. Postcuring produced specimens which were more stable over time. The continued crosslinking on non-postcured specimens can greatly complicate experimental evaluation because of the changing material properties ([36] [37]). The postcure was also expected to simulate the processes which would occur in a bridge deck exposed to a hot summer sun for several weeks. The stabilized samples were thus expected to be more

---

<sup>1</sup>Flexolith is a registered trade name of the Tamms Company, VA

representative of an actual bridge deck system.

### 3.3.3 Specimen conditioning

Environmental factors can seriously affect bond performance. Except for controls, all the specimens were conditioned under prescribed temperature and moisture conditions to determine the effects on bond durability. The environmental conditioning matrix is shown in table 3.1.

For environmental conditions: 30°C [86°F], 98% RH; 45°C [113°F], 98% RH and 60°C [140°F], 98% RH, distilled water was poured into each of the three water baths (size of 345 × 300 × 175 mm) to a level of approximately 51 mm. A CPVC pipe with a height of 76 mm was placed into each chamber serving as a support to keep the specimens above the water level. The specimens were stacked directly on the supports in layers. Between each layer, strips were placed to prevent the specimen layers from touching, which will also allow the moisture to enter the overlay surface of the specimens.

The freeze-thaw conditioning cycle was 60°C [140°F], 100% RH for 20 hours and -25°C [-13°F] for 4 hours. The specimens were completely submerged in water in a plastic container. The container was then covered and placed in an oven at 60°C [140°F] for 20 hours. After 20 hours, the specimens were moved out of the container, wrapped in plastic and kept in a freezer at -25°C [-13°F] for four hours. In this manner, the specimens were moved between the oven and freezer each day, with each cycle taking one day to complete.

The salt water soak conditioning cycle involved immersion in a 6% NaCl (by weight) solution at 60°C [140°F] for six days and followed by one day drying at room temperature. The specimens were completely submerged in a 6% NaCl solution in a polypropylene container. The container was covered and placed in an oven at 60°C [140°F] for six days. The specimens then were removed from the container and dried for 24 hours. Other specimens

were placed in an oven at  $60^{\circ}\text{C}$  [ $140^{\circ}\text{F}$ ], at very low relative humidity to determine the effect of elevated temperature exposure.

### 3.3.4 The auxiliary adherend bonding

After scheduled aging times, the specimens were removed from their environmental chambers. Two auxiliary aluminum bars (cut from the webs of the beam scrap, as shown in figure 3.1) were bonded onto the polymer concrete surface using Flexolith 216R to provide sufficient energy storage to cause debonding. It is important that the bond to the aluminum beam be sufficiently strong to avoid failures at this site. Sand paper with a grit size of 200 was used to scrub the auxiliary aluminum surface until contamination could not be seen and the surface appeared to be smooth and bright. The sandwich specimens were placed in an oven at  $60^{\circ}\text{C}$  for 24 hours to cure the secondary bond before being tested.

### 3.3.5 Testing

#### Precrack

To reduce the influence of viscoelasticity, the sandwich specimens were conditioned in dry ice for 5 hours to achieve a uniform temperature before testing. Because of the short testing time and the massive nature of the specimens, the MMF testing was assumed to be conducted at  $-33^{\circ}\text{C}$ , the temperature of dry ice. Then an initial crack length of "a" was introduced at the primary interface by three-point bending, as shown in figure 3.2. The notch was centered between the two supports, and the moment was focused at the center by a reduction of the support separation distance to 150 mm. A relatively high crosshead speed of 15 mm/min was used to produce the initial debonds. The type and direction of stresses at the notch tip prior to crack growth is shown in figure 3.2 as well. Crack initiation was observed visually from the sample with the use of a magnifying flashlight. White paint was placed on both sides to make the crack tip readily visible. Loading jumps at a certain displacement of the crosshead provided evidence of debond initiation as well. The crack

arrest length was controlled to be approximately 30 mm.

### Modified MMF test

A modified mixed mode flexure (MMF) test geometry, as illustrated in figure 2.4, was selected for the interfacial fracture toughness testing of this material system. The MMF tests were performed on the pre-cracked samples to determine the critical strain energy release rate. As the name of the test implies, the debond at the interface is under a combined opening and shear mode loading. In the standard MMF test, the applied load is centered between the two supports. Because of the dimensions on the notched specimens and the desire to increase the length available for debonding, the load was located at the quarter point as shown in figure 2.4.

The MMF testing was conducted on an Instron 4505 universal test frame controlled by a LabVIEW<sup>2</sup> program. The testing rate was 1 mm/min. When the crack began to propagate, the crosshead was held. After the crack arrested, the crack lengths on both sides of the sandwich specimen were recorded, and the average value was used for data analysis. In most cases, the critical load was the maximum load. In some situation, even after the crack began to propagate, the load kept increasing, but the slope of the load vs. displacement decreased. In this case, the critical load was defined when the load vs. displacement curve began to change the slope. The specimen was unloaded to finish one cycle. Three to four cycles for crack propagation can be obtained per end. Then the specimen was reconditioned in dry ice for two hours and retested on the other end.

## 3.4 Results and Discussion

The compliance method [7] [38] was used to determine the critical strain energy release rate for the bond between the polymer concrete overlay and the aluminum substrate. Using

---

<sup>2</sup>LabView is a trademark of National Instruments Corporation, TX

$$G = \frac{1}{2b} P^2 \frac{\partial C}{\partial a} \quad (3.1)$$

where  $P$  is the force at the onset of crack growth,  $a$  the crack length,  $b$  the specimen width, and  $C$  the compliance of the test specimen, which can be determined experimentally.

The data points obtained from the specimens with the same aging condition and aging time were fitted using the compliance method in the MMF analysis, as shown in figure 3.3. For a given crack length,  $dC/da$  could be computed, and the strain energy release rate  $G_c$  could be obtained from the measured critical load.

A typical MMF loading-unloading plot is displayed in figure 3.4. Only the first cycle had a large zero offset effect, after which the material seemed to settle. Such effects are common in systems which undergo plastic deformation, but in this case, the deformation of the aluminum remained within the calculated elastic range. One possible reason for the zero offset is that some cracks initiated between the adhesive and the silica aggregate during the test. The slope of the load vs. displacement curve was consistent from the second cycle on, so no information for the first cycle was used. Usually the data from the last run were ignored because the crack tip was too close to the loading point. Test results for the aged and control specimens are shown in figure 3.5.

$G_c$ , the critical strain energy release rate, is a material system property which should be independent of initial crack length "a". The  $G_c$  results exhibited relatively high variability for physical property measurements. Possible reasons for the scattered data are geometric variations between specimens, non-uniform crack fronts, voids of non-homogenous coating, uncertainty in debond length, and some uncertainty on the determination of the critical loading from the load versus displacement curve. The test technique had been refined, so the geometric variations might have greatest influence.

In spite of considerable scatter in the data, downward trends in toughness are seen with

increased aging time, see figure 3.5. The initial results have shown small reductions in bond toughness following 2 months exposure to freezing-thawing and salt water soak cycles. After 6 months of exposure to elevated temperatures and humidities, a noticeable loss in bond toughness is apparent. The testing results suggest that the interfacial toughness was degraded by the exposure conditions. For most specimens, crack growth occurred close to the interface between the PC and Al. For the specimens aged in the following environmental conditions: 60°C, 98% RH, aged for 6 months; 60°C, dry, aged for 6 months; 45°C, 98% RH, aged for 12 months; salt water soak, aged for 12 months; aging appears to affect the silica/epoxy bond as well. Because cracking occurred within the polymer concrete and along the interface, it was not possible to obtain the true fracture toughness value of the PC/Al bond. The color of specimens aged at 60°C changed significantly, suggesting that the properties of polymeric components in the coating had changed.

Figure 3.6 shows the experimentally determined G values by the compliance method with G values determined by FEA and the analytical equation. The G values obtained from compliance method were the highest. One possible reason is due to the test methods. The elastic modulus used in the analytical solution and FEA was from the tensile test, while the real fracture test was bend type test. Although the same crosshead rate was used in the testing, the strain rates of the specimen were different, which would affect the measurement of the elastic modulus.

## 3.5 Post-failure Surface Analysis

### 3.5.1 Scanning electron microscopy (SEM)

In studies of adhesive bonding, failure analysis is critical. SEM, a very common technique, was applied in the identification of the failure locus.

Figure 3.7 shows after failure, some of the grinding marks had trapped adhesive, thus,

indicating that mechanical interlocking has taken place. Increased surface roughness can result in subsequent mechanical bond between the overlay and the substrate. From figure 3.7, the grinding marks on the original aluminum surface are visible. Both the extrusion and crack propagation directions are perpendicular to the direction of the grinding grooves. Figure 3.8 shows the machine marks and the polymer failure on the polymer concrete side, as well. Figure 3.7 and 3.8 demonstrate that the two failed surfaces are very similar. From this, we concluded that the actual failure locus was very close to the aluminum surface, but a small amount of adhesive was left on the aluminum.

### 3.5.2 X-ray photoelectron spectroscopy (XPS)

X-ray photoelectron spectroscopy (XPS) [36], was employed to identify the chemical composition of the surface regions. It can provide a very good qualitative and quantitative elemental analysis of a surface. XPS was performed using a Perkin Elmer model 5400 x-ray photoelectron spectrometer. The surface sampling depths is around  $40\text{-}50 \times 10^{-10}$  m. In XPS spectra, x axis presents the binding energy and y axis presents the number of electrons detected per unit energy. XPS survey spectra of the failure surfaces are shown in figure 3.9, (polymer concrete side) and figure 3.10, (aluminum substrate side), respectively. Table 3.2 shows the results of elemental analysis, and the data are the average values of two survey spots.

XPS results revealed that the two opposite failure surfaces consisted mainly of carbon and oxygen. On the aluminum side, however, the carbon peak was different from that of the polymer concrete side, which means the failure is not completely cohesive. The Al from  $Al_2O_3$  and Al are found on the failed aluminum side. Very small amounts of Al, Zr and S, which originate from the aluminum, were found on the polymer concrete surface. The percentage of C and N, were similar on both sides, which indicates that some adhesive was left on aluminum side as well.

The presence of Zr and S may be due to the proprietary surface pretreatment. Visual inspection of the controls and the aged specimens failure surfaces suggested failure close to the interface. A lot of epoxy bumps were left on the aluminum surface. These appear to be bubbles on these specimens. There is considerable variability in how many such bubbles occur on a given specimen. This might be one explanation for the fracture test data scatter.

### 3.6 Summary and Conclusions

This study was initiated to evaluate the durability of the polymer concrete coating to the aluminum bridge decks. A modified mixed-mode flexure fracture test was employed in this research. The method was effective for evaluating the durability of polymer concrete bonds to aluminum bridge decks. The downward trends in the critical strain energy release rate showed that the degradation of fracture toughness increased with increasing aging time. However, for some specimens aged at 60°C with/without humidity, the epoxy/aggregate bond was degraded over time, which resulted in crack extension within the coating. Bond fracture toughness could be not determined for the specimens because failure occurred within the coatings.

Both visual observation and SEM showed that the failure locus of the MMF specimens was close to the interface. Only a small amount of epoxy was left on the aluminum substrate. For those specimens aged at 60°C with/without humidity, failures within the coating was observed. It seems that the degradation of polymer and polymer/aggregate sufficiently prevented the interfacial failure at the Al/PC bond.

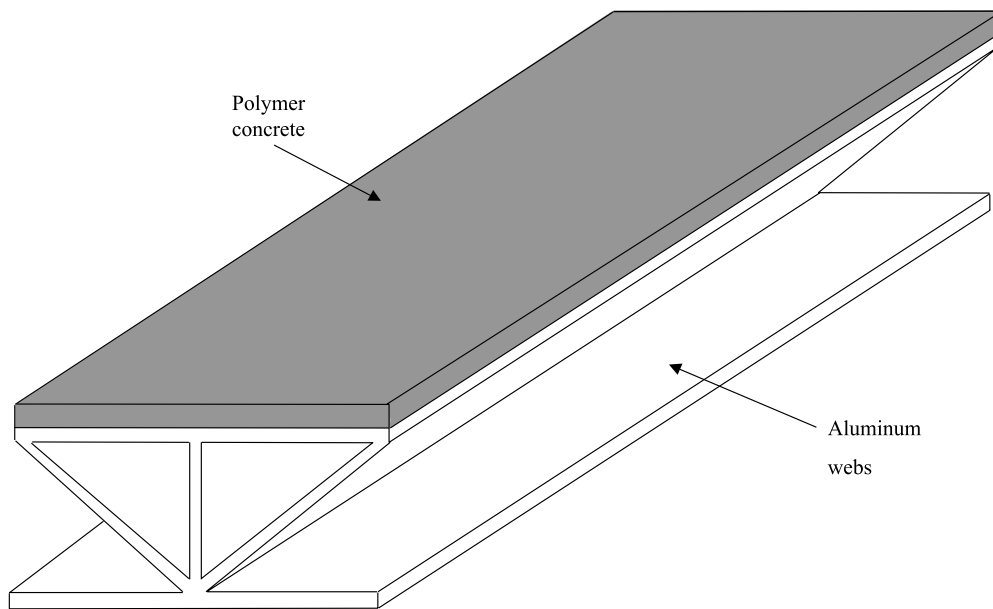


Figure 3.1: Aluminum bridge deck beam

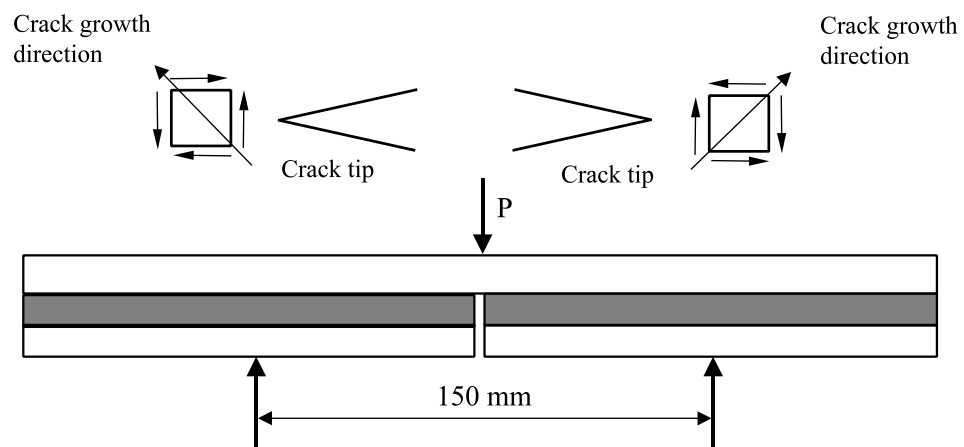


Figure 3.2: Three-point bending used to initiate the debond at the primary (upper) interface

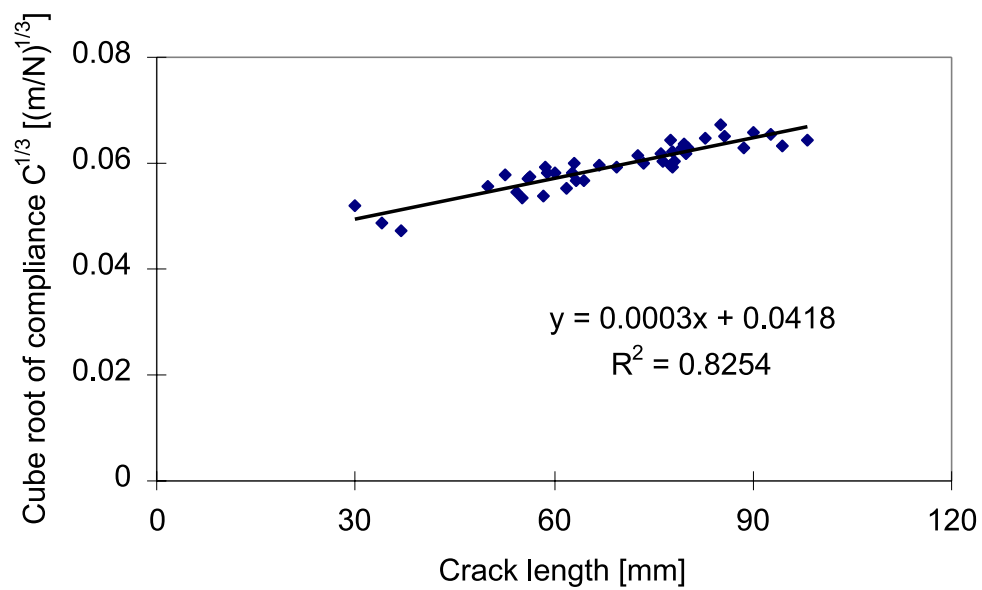


Figure 3.3: Data fit for typical compliance method (Data from the specimens with the same aging condition and aging time)

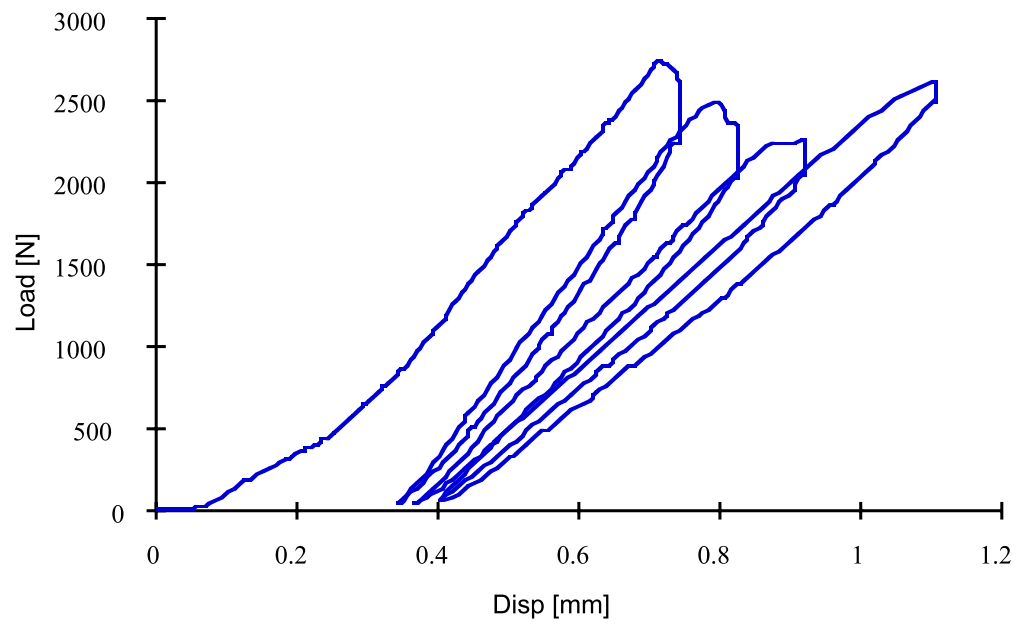


Figure 3.4: Plot of typical MMF loading-unloading curve

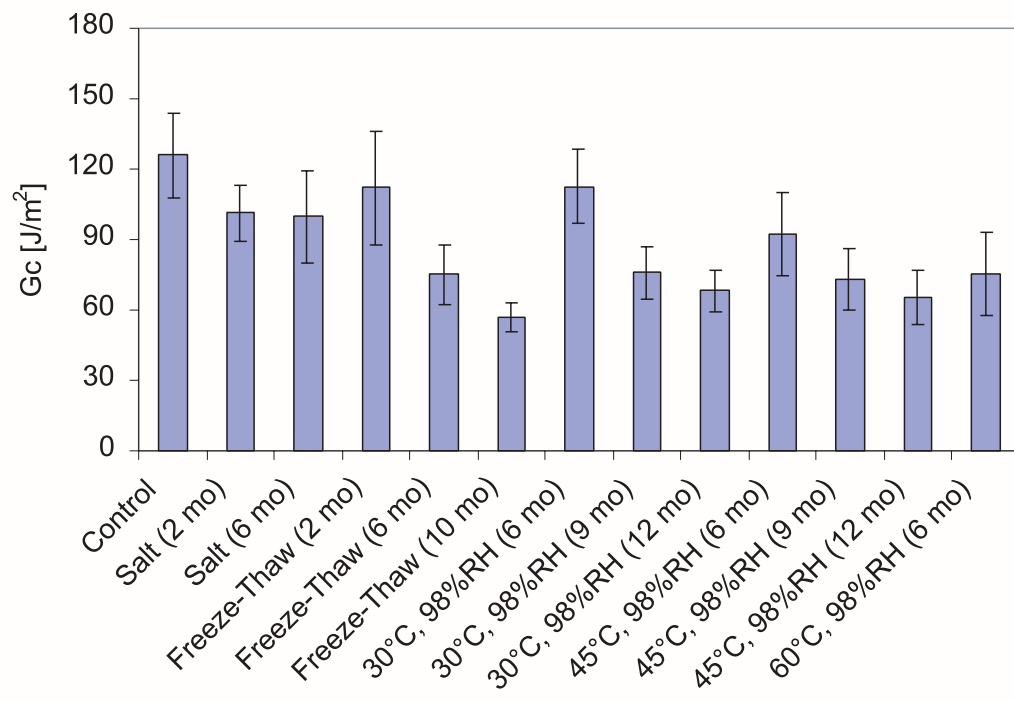


Figure 3.5: Critical energy release rate for control and aged specimens, showing numerical averages and error bars with  $\pm\sigma_{n-1}$

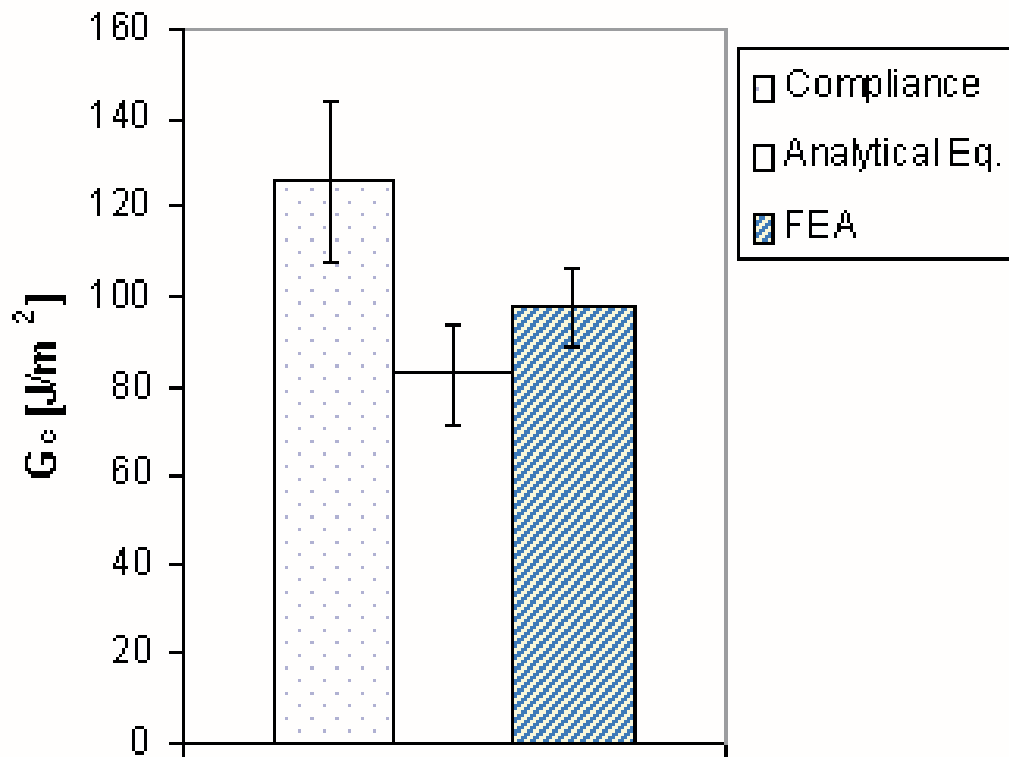


Figure 3.6: Comparison of  $G$  (for controls) from compliance method, FEA, analytical equation, showing numerical averages and error bars with  $\pm\sigma_{n-1}$

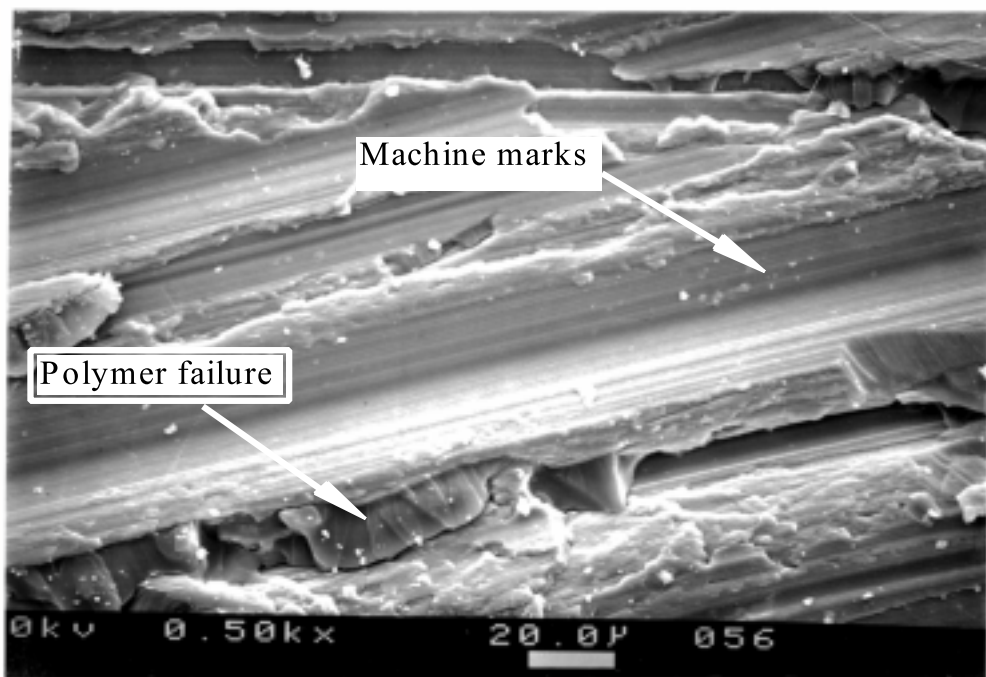


Figure 3.7: Failed aluminum surface

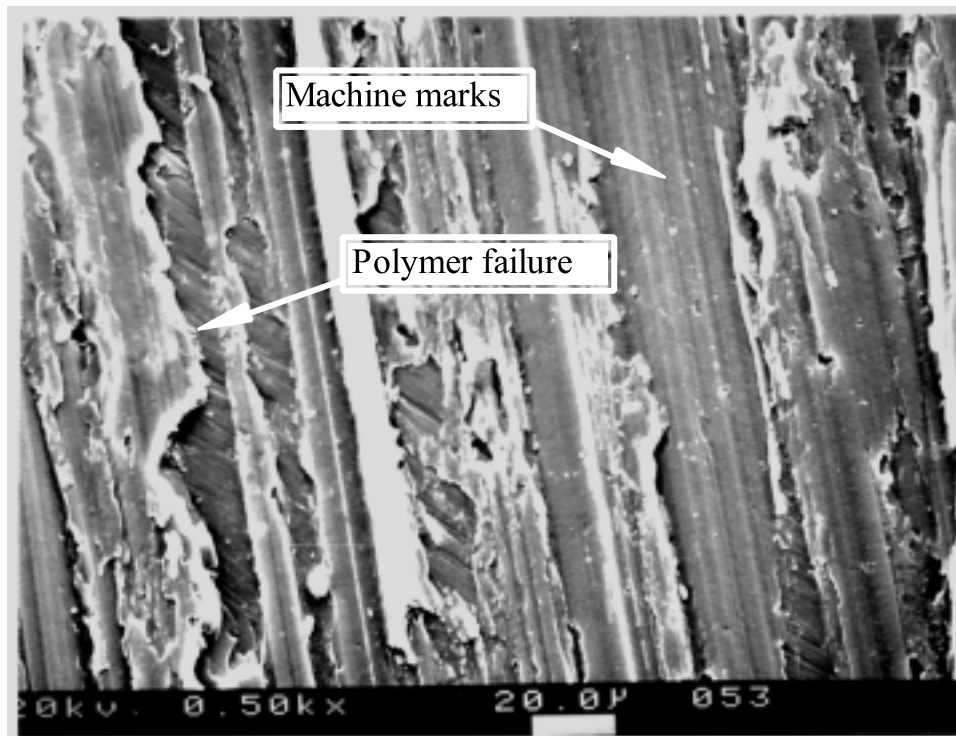


Figure 3.8: Failed polymer concrete surface

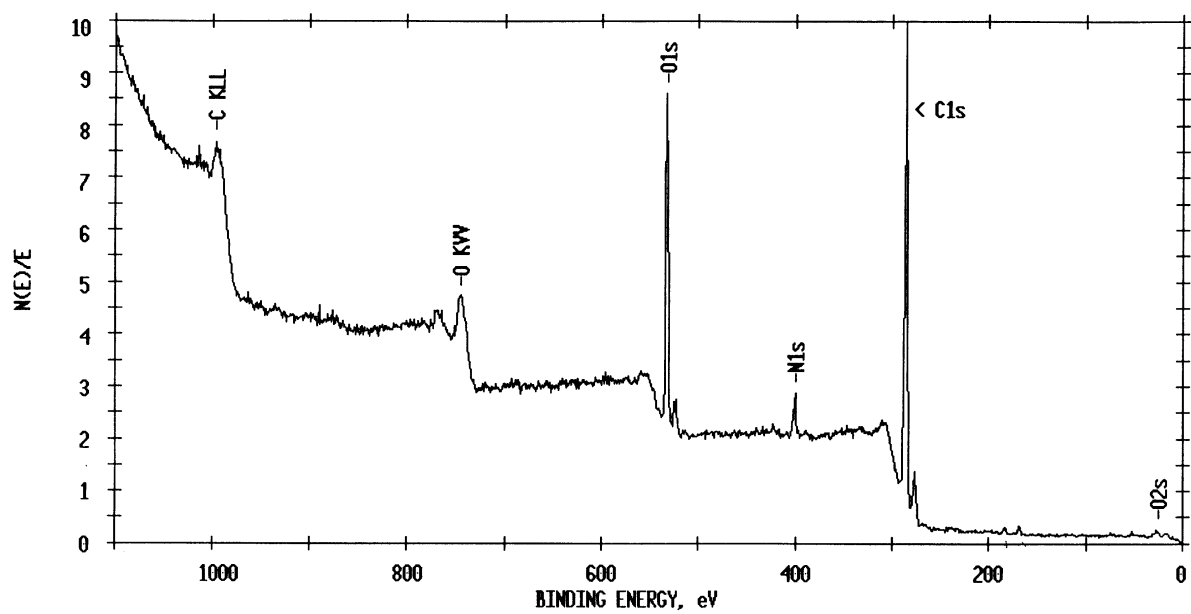


Figure 3.9: XPS survey spectrum of failed polymer concrete surface

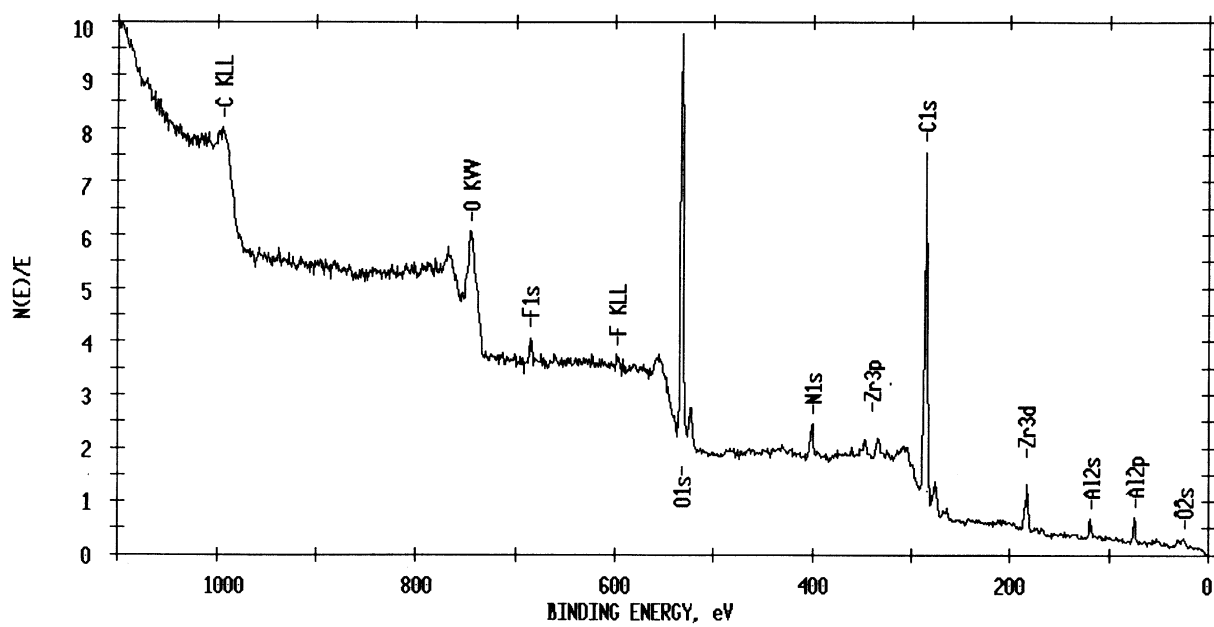


Figure 3.10: XPS survey spectrum of failed aluminum surface

Table 3.1: Environmental conditioning matrix

	As received	30° C 98% RH	45° C 98% RH	60° C 98% RH	Freeze-thaw	Salt water soak	60° C dry
Controls	20						
2					6	6	
6		6	6	6	8	7	7
9		6	6	6	8		
12		6	6	6			6

Table 3.2: XPS element analysis of different surfaces

Element	Neat postcured epoxy sample surface (%)	Failed PC surface controls (%)	Pretreated Al surface (%)	Failed Al surface, con- trols (%)
C $1_s$	79.8	75.2	52.7	62.4
O $1_s$	14.2	18.7	32.5	27.3
N $1_s$	4.8	4.2	1.9	4.2
Al $2_p$	0	0.5	4.8	3.8
Si $2_p$	1.2	<0.1	<0.1	<0.1
S $2_p$	0	0.5	<0.1	0.3
F $1_s$	0	<0.1	5.7	1.1
Zr $3_d$	0	0.2	4.8	1.0

# Chapter 4

## Material Characterization

### 4.1 Introduction

The analytical and numerical solutions of the MMF specimens are dependent on the properties of the materials. The properties of the neat polymer and the polymer concrete at room temperature and  $-33^{\circ}\text{C}$ , such as elastic modulus and Poisson's ratio, need to be investigated.

### 4.2 Polymer Concrete

#### 4.2.1 Shear modulus

##### **Bending testing for shear modulus**

The shear modulus of the polymer concrete was calculated using a three-three layer composite model. The prediction was compared with the bending experiment results.

The three point bending of a bonded beam proposed by Moussiaux [39] was conducted to determine the polymer concrete properties. Moussiaux derived an expression for the beam deflection as a function of the adhesive shear modulus, as given in equations (4.1 - 4.5). The basic geometry of the specimen, illustrated in figure 4.1, consists of three layers of

two different materials. The outer layers are 6063-T6 aluminum and the inner layer is the polymer concrete. The specimen was made by bonding an additional aluminum layer onto the surface of the original specimen which consisted of one layer of aluminum and one layer of polymer concrete. Thicknesses of the three layers are as follows (from the top to bottom):  $h$  (10.6 mm),  $t$  (6.8 mm),  $h$  (10.6 mm) and specimen width is  $b$  (51 mm).

$$\alpha^2 = 3 \frac{G_a}{E} \left( \frac{L}{a} \right)^2 \frac{\left( 1 + \frac{2t}{h} \right)^2}{\frac{t}{h}} \quad (4.1)$$

$$\tilde{\alpha} = \alpha \gamma \quad (4.2)$$

$$\gamma^2 = 1 + \frac{1}{3 + \left( L + \frac{2t}{h} \right)^2} \quad (4.3)$$

$$\delta = \beta \frac{PL^3}{2Eb(h+t)^2} \quad (4.4)$$

$$\beta = \left( 1 + \frac{t}{h} \right)^3 \left( 4 \left( 1 - \frac{1}{\gamma^2} \right) + \frac{3E}{G} \left( \frac{h}{L} \right)^2 + \frac{12}{\gamma^2} \left( \frac{1}{\tilde{\alpha}^2} - \frac{\tanh \tilde{\alpha}}{\tilde{\alpha}^3} \right) \right) \quad (4.5)$$

$E$  (68 *GPa*) is the elastic modulus of the aluminum;  $G$  (26 *GPa*) is the shear modulus of the aluminum;  $G_a$  is the shear modulus of the polymer concrete;  $d$  is the deflection at the loading point;  $P$  is the applied load. Bending testing was conducted at -33°C with a crosshead rate of 1 mm/min to reduce the viscoelastic behavior of the polymer concrete. A typical load vs. deflection curve is illustrated in figure 4.2. The solid line represents the experiment results, and the dashes line is the trendline. The shear modulus of the polymer concrete coating was 5.8 *GPa* from the experiment.

### Theoretical analysis

To model the elastic properties of polymer concrete, the elastic properties and volume fraction of the components must be known. The polymer concrete consists of an epoxy binder

and the silica aggregates. The elastic modulus and Poisson's ratio of the neat polymer were 2.8 *GPa* and 0.35 at -33°C, respectively based on tensile tests. The Young's modulus, shear modulus, Poisson's ratio, and bulk modulus of the silica aggregate were estimated as  $E_p = 40$  *GPa*,  $G_p = 16.4$  *GPa*,  $\nu_p = 0.22$ ,  $K_p = 23.8$  *GPa*, respectively [24]. The filler (silica aggregate) volume fraction,  $V_f$ , reported by Reynolds was 0.70.

A variety of approaches have been proposed to develop relationships to predict the Young's modulus, shear modulus, Poisson's ratio and bulk modulus of particulate composites [40]. The Voigt and Reuss approaches give upper and lower bounds of the elastic properties of a composite. These approaches are based on the assumption that each phase component is subjected to either the same stress or the same strain (4.6, 4.7).

Voigt (constant strain)

$$[C_c] = V_f [C_f] + V_m [C_m] \quad (4.6)$$

Reuss (constant stress)

$$[S_c] = V_f [S_f] + V_m [S_m] \quad (4.7)$$

$[C]$ s are the elastic stiffness arrays for the composite, the filler, and the matrix respectively;  $[S]$ s are the compliance constant arrays for the composite, the filler and the matrix respectively.  $V_f$  is the filler volume fraction;  $V_m$  is the matrix volume fraction.

Expressions for the elastic moduli of two heterogeneous materials have been given by Hashin [41] based on the variational theorems of the theory of elasticity and on a concentric-spheres model. An important assumption for this analysis of the heterogeneous materials is that the fractional volume of the inclusions is very small and that the particles do not interact. Although the assumptions are not strictly true in this case, the preliminary estimates were based on this model (equations 4.8 - 4.11).

$$K = K_m \left( 1 + \frac{3(1 - \nu_m) \left( \frac{K_f}{K_m} - 1 \right) V_f}{2(1 - 2\nu_m) + (1 + \nu_m) \left[ \frac{K_f}{K_m} - \left( \frac{K_f}{K_m} - 1 \right) V_f \right]} \right) \quad (4.8)$$

$$G = G_m \left( 1 + \frac{15(1 - \nu_m) \left( \frac{G_f}{G_m} - 1 \right) V_f}{7 - 5\nu_m + 2(4 - 5\nu_m) \left[ \frac{G_f}{G_m} - \left( \frac{G_f}{G_m} - 1 \right) V_f \right]} \right) \quad (4.9)$$

$$E = \frac{9KG}{3K + G} \quad (4.10)$$

$$\nu = \frac{3K - 2G}{2(3K + G)} \quad (4.11)$$

Subscripts  $m$  and  $f$  refer to the matrix and the filler, respectively.  $E$  is the elastic modulus;  $G$  is the shear modulus;  $\nu$  is Poisson's ratio;  $K$  is the bulk modulus;  $V_f$  is the filler volume fraction. The three models used to predict the shear modulus of polymer concrete and the test results are presented in figure 4.3. Using the components' properties, Hashin's model appears to fit the experiment result reasonably well. This was not the case for Poisson's ratio, as shown in figure 4.4. Two possible reasons are that the void formation would lower the measured  $\nu$ , and the accuracy of the  $\nu$  measurement.

## 4.2.2 Stress-strain testing

### Specimen dimension

Tensile property measurements were conducted using an Instron 4505 universal test frame at a constant crosshead rate of 1 mm/min. The shape of the aggregate in the polymer concrete was irregular, and the diameter of the particles varied from 0.1 mm to 4.5 mm. Since the size of the aggregate was relatively large, no standard dog-bone specimen was appropriate for these composite materials. A scaled-up version of the standard ASTM D638-96 dog-bone specimen for plastic materials was used to measure the elastic modulus of the PC. The scale factor used was 2.6, and the final dimensions are shown in figure 4.5.

In figure 4.5,  $G$  is the gage length (102 mm),  $A$  the reduced section length (203 mm),  $B$  the length of grip section (64 mm),  $L$  the over all length (330 mm),  $W$  the width (34 mm),  $C$  the width of grip section (51 mm),  $T$  the thickness (13 mm), and  $R$  the radius of fillet (76 mm).

### Sample fabrication

Equal volumes of the Flexolith 216 R A and B components were mixed thoroughly in a clean container using an electric drill fitted with a stirring rod. The silica aggregate (2.35 times the volume of the mixed Flexolith) was stirred into the epoxy. To achieve a uniform mixture, effort was taken to wet all the aggregate prior to casting. The dog-bone specimens were cured for a minimum of seven days. Because a large number of voids were visually observed on the surface of the PC, it is reasonable that some voids existed within the specimen. Since Reynolds Metals Company has been able to fabricate specimens more reproducibly, Reynolds fabricated the test specimens in rubber molds provided by Virginia Tech.

More than two weeks after fabrication, a number of polymer concrete dog-bone specimens cast by Reynolds Metals Company were tacky to the touch. Similarly, Virginia Tech specimens were tacky after two weeks for a batch that was mixed quickly to avoid air bubble formation. The specimen tackiness or incomplete cure is probably due to insufficient mixing. The thicknesses of the PC dog-bone specimens are 13.2 mm, which is more than the 12.7 mm required by the scaled up test specimen thickness. Air bubble voids were also observed in the specimens.

### Tensile testing

In measuring Poisson's ratio, one extensometer with a 25 mm gage length was used in the axial direction and another with a 12.7 mm gage length in the transverse direction on axially loaded dog-bone specimens. The elastic properties at room temperature and  $-33^{\circ}\text{C}$

are shown in table 4.1.

### 4.2.3 Stress relaxation testing

A bend type test was utilized to study the stress relaxation property of the PC coating using an Instron 4505. The tests were run on the sandwich sample without notch at RT and  $-33^{\circ}\text{C}$ . It was found that when displacement was held constant, 36 percent of original load dropped in ten minutes at room temperature, as shown in figure 4.6. Only 8 percent of the original load dropped in ten minutes at  $-33^{\circ}\text{C}$ , as shown in figure 4.7. The same test was repeated on aluminum beams to verify the stability of the load frame. The results of the test on aluminum indicated negligible time dependence in the aluminum/load frame time dependence and confirm the substantial time dependences of elastic modulus of the polymer concrete in the sandwich beams at room temperature.

## 4.3 Properties of Neat Polymer

### 4.3.1 Thermal gravimetric analysis (TGA)

Thermal gravimetric analysis (TGA) is a study of the change in mass of a material under various temperature and pressure conditions [36]. TGA was conducted on a postcured resin sample using a TA Instruments TGA 2950 in a nitrogen environment at atmospheric pressure. The temperature was ramped from  $25^{\circ}\text{C}$  to  $700^{\circ}\text{C}$  at a rate of  $10^{\circ}\text{C}/\text{min}$ . The TGA results demonstrated that the epoxy lost 2 percent of the original mass at  $168^{\circ}\text{C}$ , as shown in figure 4.8. A conclusion was made that the epoxy began to decompose at around  $168^{\circ}\text{C}$ .

### 4.3.2 Differential scanning calorimetry analysis (DSC)

Glass transition is an important property of a polymer, and whether a polymer is in a glassy or rubbery state depends on whether its application temperature is above or below its glass transition temperature. The glass transition temperature of a polymer is rapidly and

conveniently determined by differential scanning calorimetry (DSC) [42]. DSC was utilized to study the glass transition temperature of the epoxy. At a temperature ramp rate of  $10^{\circ}\text{C}/\text{min}$  using a TA Instruments DSC 2920, the  $T_g$  of a post-cured (cured at  $60^{\circ}\text{C}$  for 24 hours) sample in a second scan was  $33^{\circ}\text{C}$ , as shown in figure 4.9.

### 4.3.3 Dynamic mechanical analysis (DMA)

To study the effects of frequency on the glass transition temperature of the material, the dynamic mechanical analyzer (DMA) was used at three frequencies. The  $T_g$  was taken to be the peak of the loss modulus,  $E''$ . Specimens were prepared using a silicone rubber mold at room temperature and postcured at  $60^{\circ}\text{C}$  for 24 hours. Specimens were tested at  $1^{\circ}\text{C}/\text{min}$  between  $-50^{\circ}\text{C}$  and  $100^{\circ}\text{C}$  to obtain the glass transition characteristics. The  $T_g$ s of the Flexolith 216 R were  $22.8^{\circ}\text{C}$ ,  $30.9^{\circ}\text{C}$  and  $35.4^{\circ}\text{C}$  using frequencies of 1, 10 and 100 Hz, respectively, as shown in figure 4.10. The activation energy was 269 KJ by calculation [43].

### 4.3.4 Thermal mechanical analysis (TMA)

#### Introduction

In the real service life of the bridge, the thermal changes can affect adhesive bonds by inducing thermal stress within the material system. The stresses could increase over a number of cycles. Residual stresses caused by thermal changes have the potential to reduce life of adhesive bonds. Debonding can be caused by thermal stresses resulting from a mismatch of the coefficients of thermal expansion (CTE) of the adhesive and substrate. To determine the coefficients of thermal expansion for the epoxy and aluminum, thermal mechanical analyzer (TMA) tests were conducted.

#### Specimen fabrication

A sample with dimensions of approximately  $17.4 \times 5 \times 3.2$  mm was cut from the cured

neat epoxy. The sample was placed under the TMA probe for the thermal expansion measurement.

### Testing and results

The coefficient of thermal expansion (CTE) of the neat epoxy was determined using a Seiko TMA 100. The testing rate was  $2^{\circ}\text{C}/\text{min}$  with a temperature range from  $-100^{\circ}\text{C}$  to  $100^{\circ}\text{C}$ . The small compressive stress used during measurement was 10 KPa. The CTEs of the epoxy were  $58 \times 10^{-6}/^{\circ}\text{C}$  and  $191 \times 10^{-6}/^{\circ}\text{C}$  below and above  $T_g$ , respectively. TMA results are shown in figure 4.11.

## 4.3.5 Solvent absorption

### Introduction

Various parameters including moisture are involved in the environmental failure of adhesive joints. Moisture has some effects on the toughness of the adhesively bonded components, and the moisture diffusion is accelerated by temperature. Internal stresses can be induced by adhesive swelling due to water uptake. It was necessary to investigate the diffusion of water and other diluents within the adhesive of interest on this project.

### Specimen fabrication

Two batches of samples were cast using silicone rubber molds at room temperature. After being held for seven days at room temperature, the samples were heated to  $60^{\circ}\text{C}$  and postcured at this temperature for 24 hours. One batch of samples with dimensions of  $100 \times 100 \times 1.5$  mm was conditioned in different humidity chambers for water absorption testing. The other batch of samples with a size of  $8 \times 6.4 \times 3.5$  mm was tested for water, acetone, DMAC, and NMP diluent absorption at room temperature.

## Testing and results

The first batch of samples were placed in environmental chambers at 30°C, 98% RH; 45°C, 98% RH; 60°C, 98% RH. Two replicates were employed for each condition. The second batch of samples was immersed in water, acetone, Dimethylacetamide (DMAC), and N-methylpyrrolidone (NMP) at room temperature, respectively. One sample was for each condition. At periodic intervals the samples were removed, dried of surface water with KIM WIPERS<sup>1</sup>, weighed on an electronic analytical balance (Model:1801MP8)<sup>2</sup>, and returned to the environmental conditioning chamber or solvent bath. To determine water solubility in the epoxy under the different conditions, the ratio of the current weight at time  $t$ , to the initial dry weight of the polymer, i.e.  $M_t/M_0$ , was plotted against  $t^{\frac{1}{2}}$ . The uptake curves for the samples conditioned in environmental chambers are linear at first and smoothly lead to equilibrium values. Figure 4.12 shows the water mass uptake for the samples. Moisture uptake was accelerated by increasing the temperature. The activation energy was 42 KJ/mol [44]. Figure 4.13 shows that the NMP is the strongest solvent for the epoxy material.

### 4.3.6 Stress-strain testing

Equal volumes of Flexolith 216R A and B components were mixed thoroughly in a sealed plastic bag (to reduce the amount of air bubbles). The mixture was then poured slowly into a dog-bone shaped silicone rubber mold before the onset of curing. After curing for seven days at room temperature, the dog-bone specimens were postcured in an oven at 60°C [140°F] for 24 hours to increase the degree and uniformity of polymerization. Since the glass transition temperature of this polymer is approximately equal to room temperature, continuing polymerization of non-postcured specimens can significantly change the material properties over time. The standard ASTM D638-96 dog-bone specimen dimensions for plastic materials were used. (see figure 4.5).

---

<sup>1</sup>Kimberly-Clark Corporation, Roswell, GA 30076-2199

<sup>2</sup>Brinkmann Instruments Co. Westbury, NY

Tensile tests were conducted on a computer controlled Instron load frame. The results are shown in table 4.2.

## 4.4 Properties of the Aluminum

### 4.4.1 Strain-stress testing

The substrate metal used for constructing the bridge beams was an extruded aluminum alloy 6063-T6. The standard ASTM B557-94 dog-bone specimen for aluminum was used to measure the tensile properties. Dogbone tensile tests, performed in the Instron 4505 at room temperature, were conducted on aluminum samples at a constant rate of 1 mm/min. The elastic modulus is 68 *GPa* and elongation is 7.2% at break. The yield stress, as determined by the 0.2% offset method was 227 *MPa*.

### 4.4.2 Thermal mechanical analyzer (TMA)

An aluminum sample with a size of 11.6×8.5×6.4 mm was cut from the bridge deck. The coefficient of thermal expansion (CTE) of the aluminum was determined using a Seiko TMA 100. The testing rate was 10°C/min with a temperature range from 0°C to 100°C. The CTE of aluminum was  $27 \times 10^{-6}/^{\circ}\text{C}$ . TMA results are shown in figure 4.14. The summary of the properties of the aluminum is listed in table 4.3.

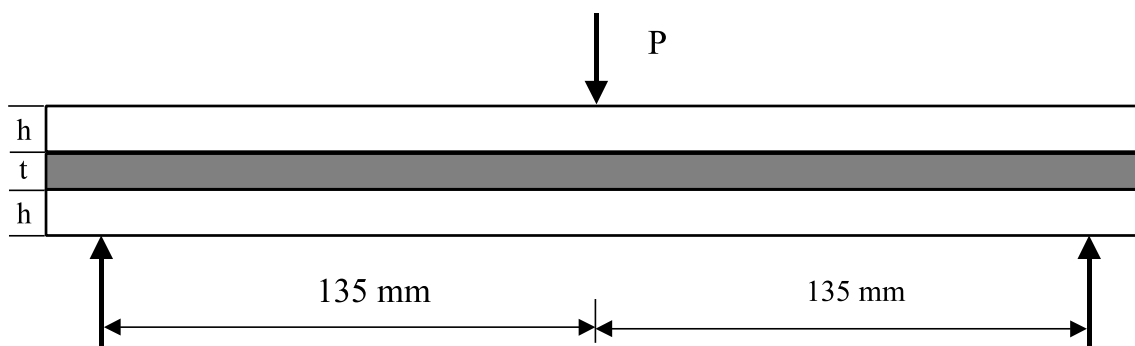


Figure 4.1: Geometry of the three-point bending test

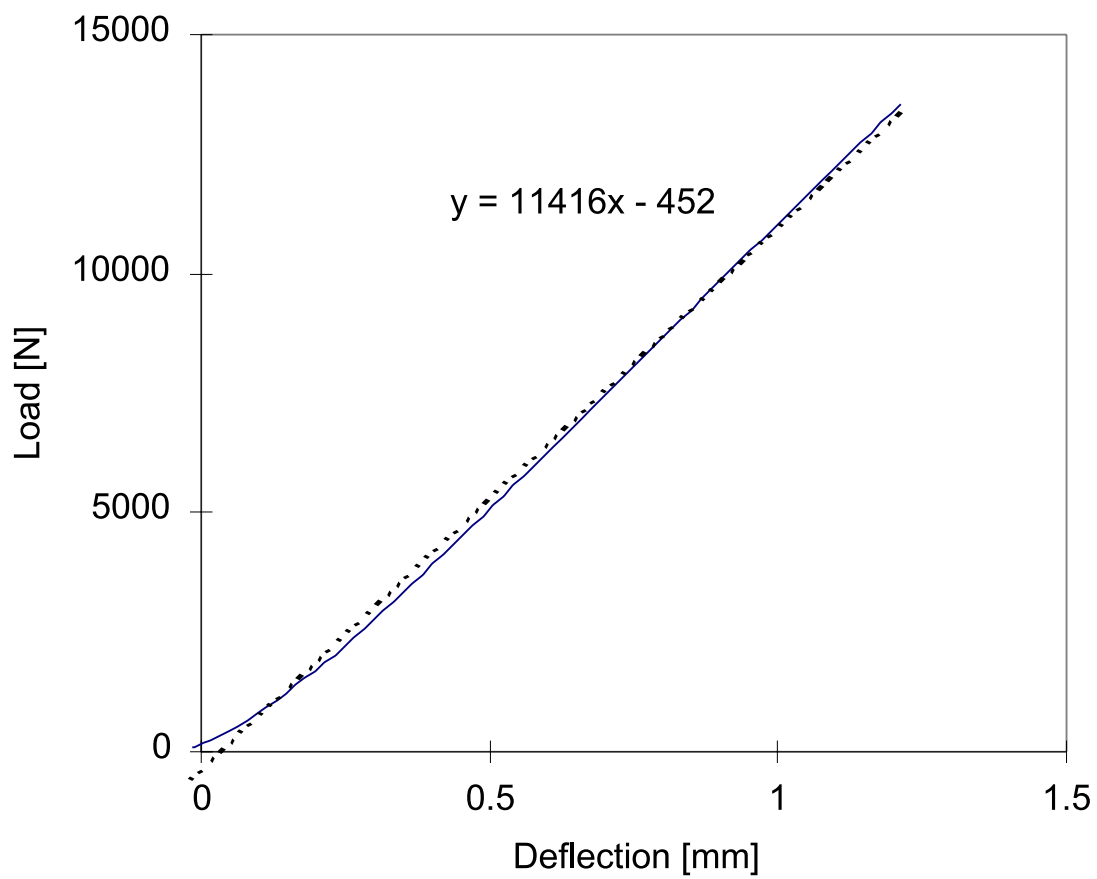


Figure 4.2: The three-point bending test results

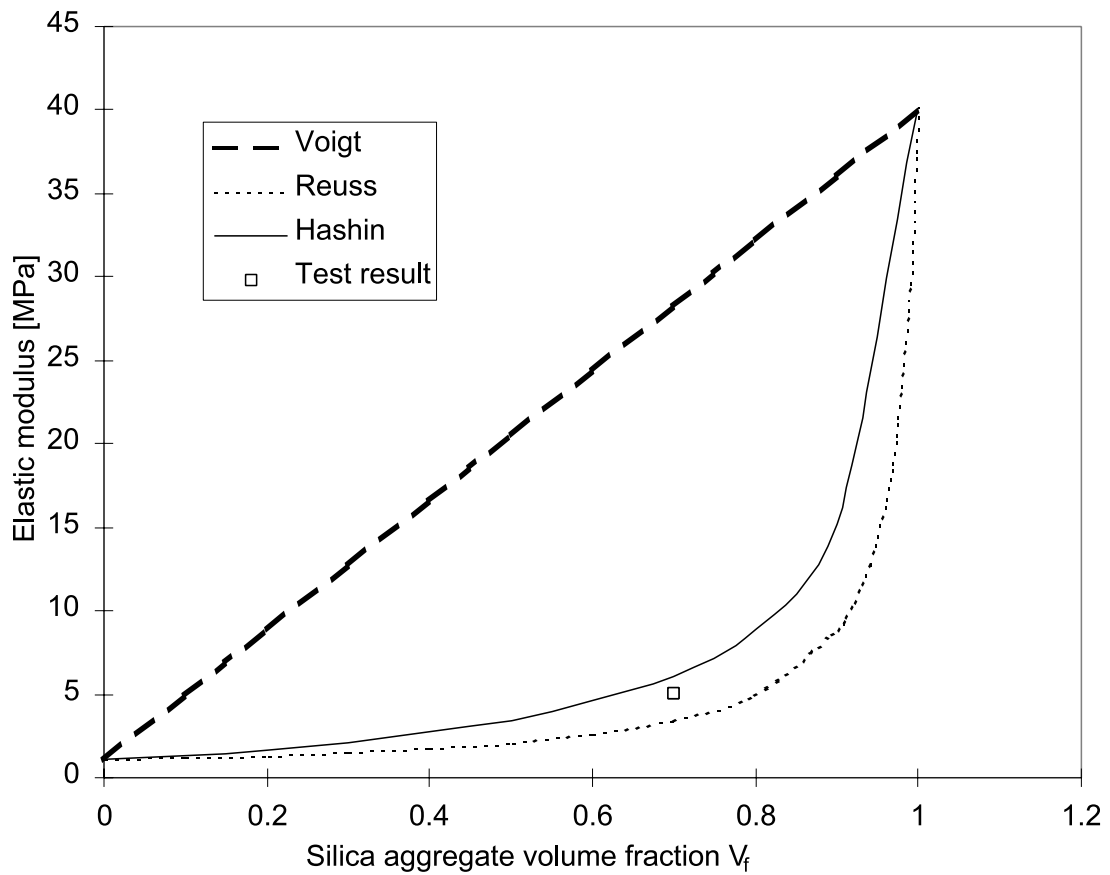


Figure 4.3: Comparison of the measured elastic modulus with predictions based on three models

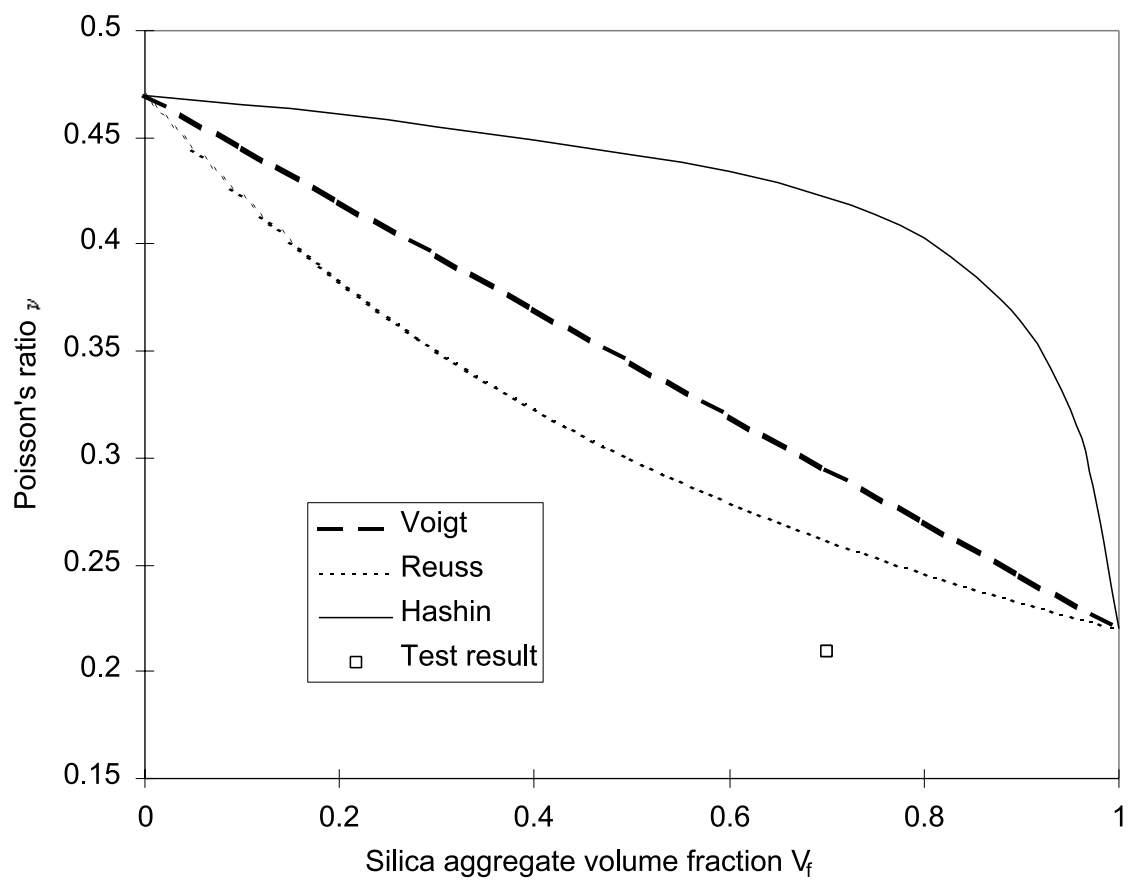


Figure 4.4: Comparison of the measured ratio with predictions based on three models

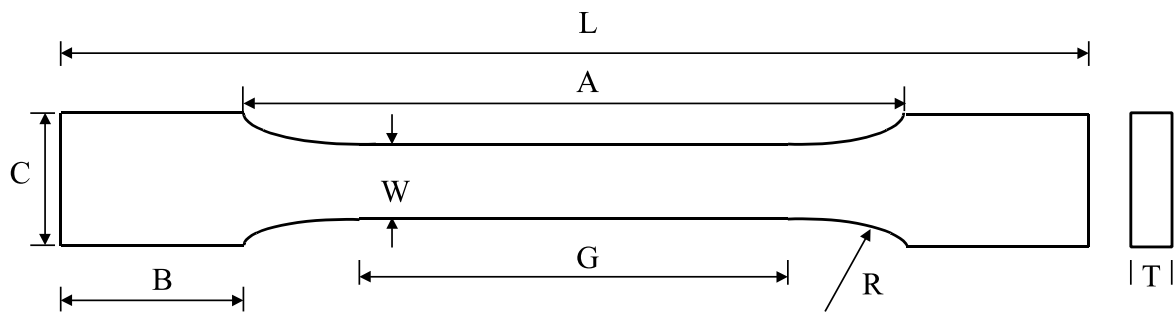


Figure 4.5: Geometry of the tensile test specimen

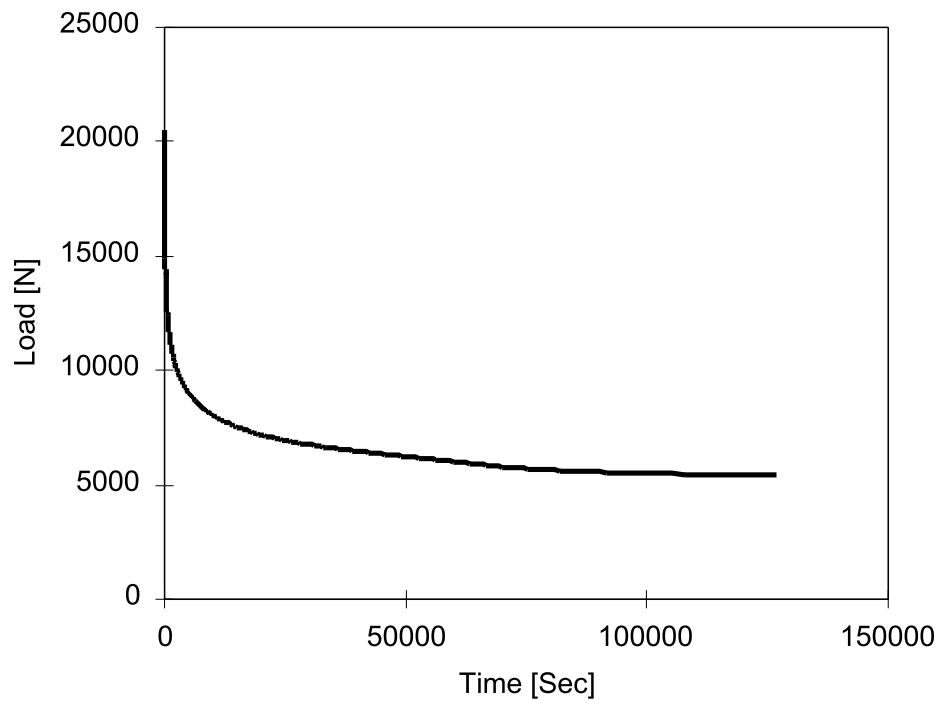


Figure 4.6: Relaxation test results for a sandwich sample at room temperature

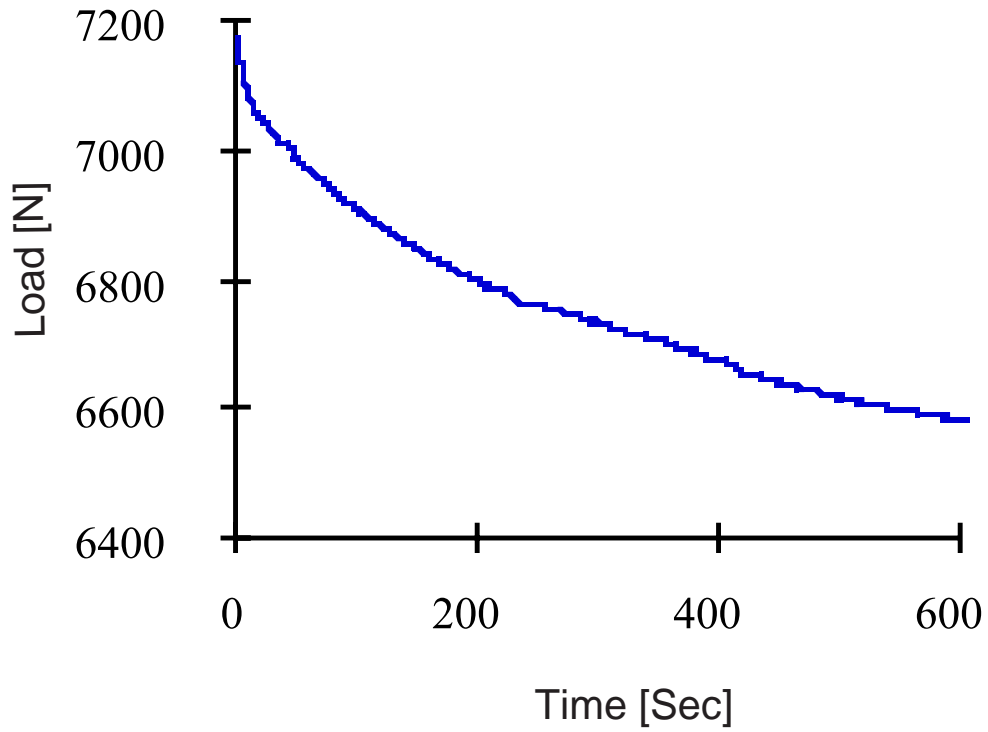


Figure 4.7: Relaxation test results for a sandwich sample at  $-33^{\circ}\text{C}$

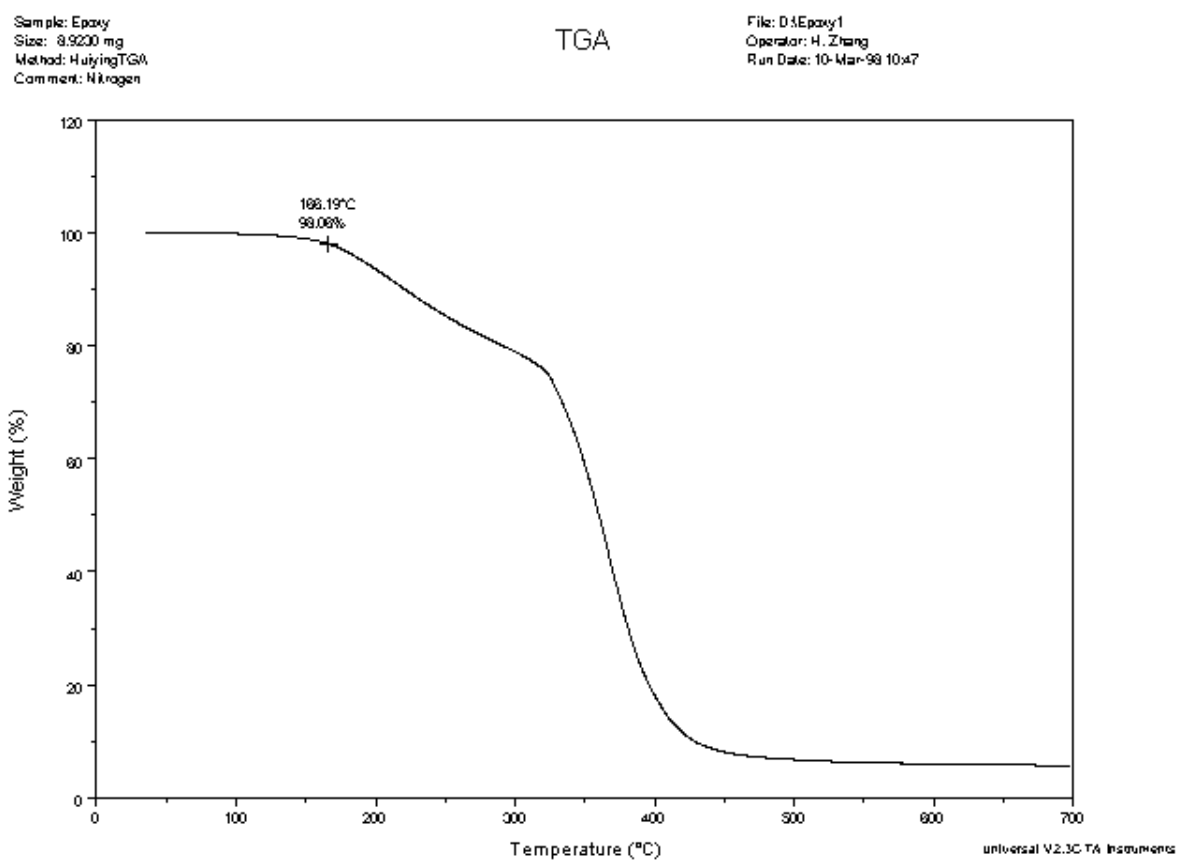


Figure 4.8: TGA data for Flexolith 216R

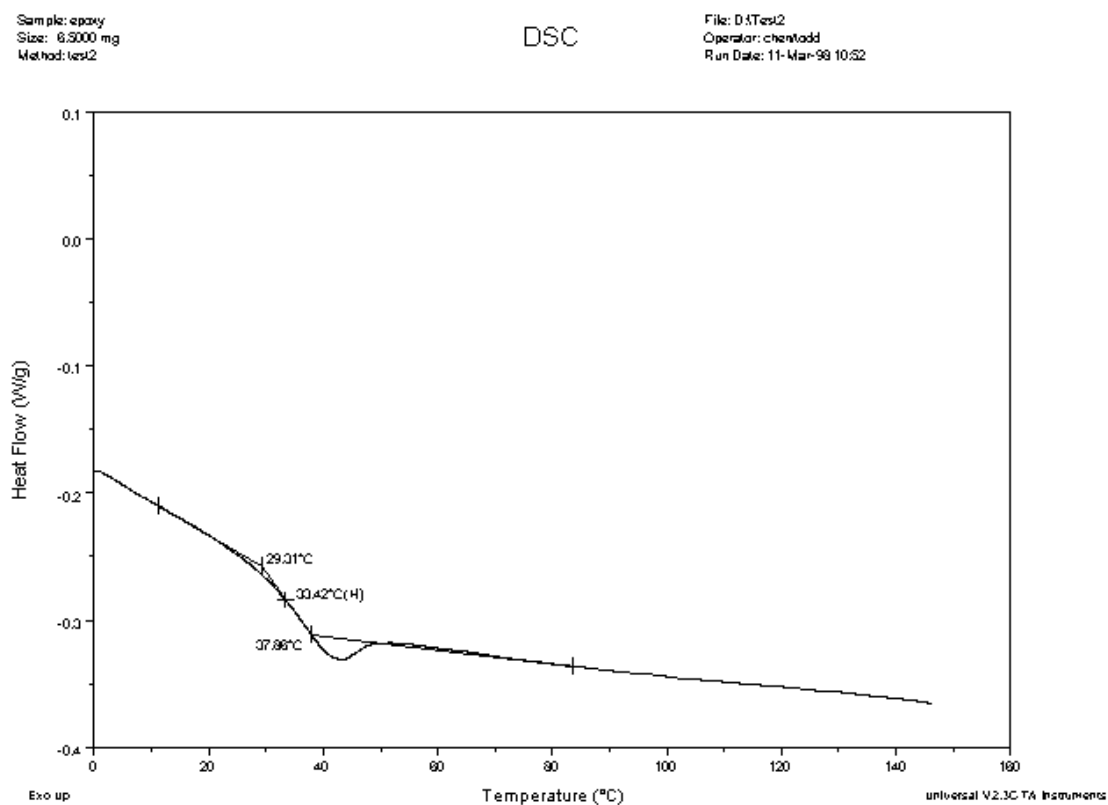


Figure 4.9: DSC data for Flexolith 216R (2nd run)

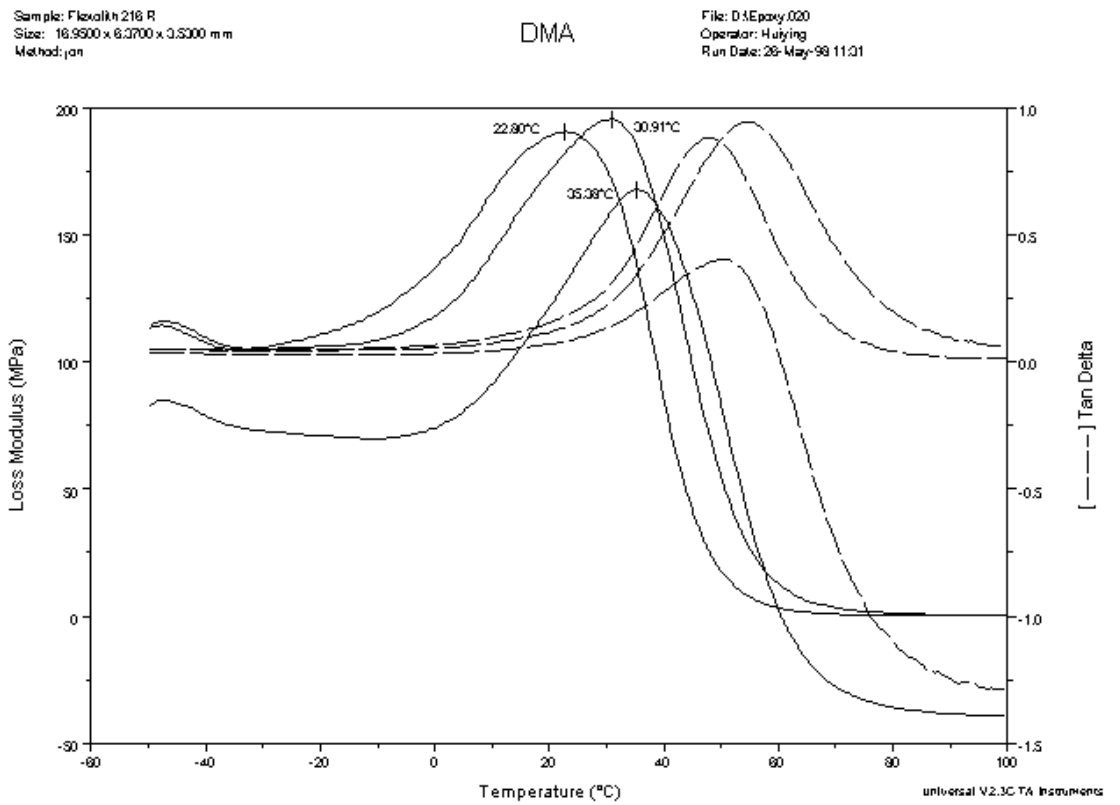


Figure 4.10: DMA data for Flexolith 216R

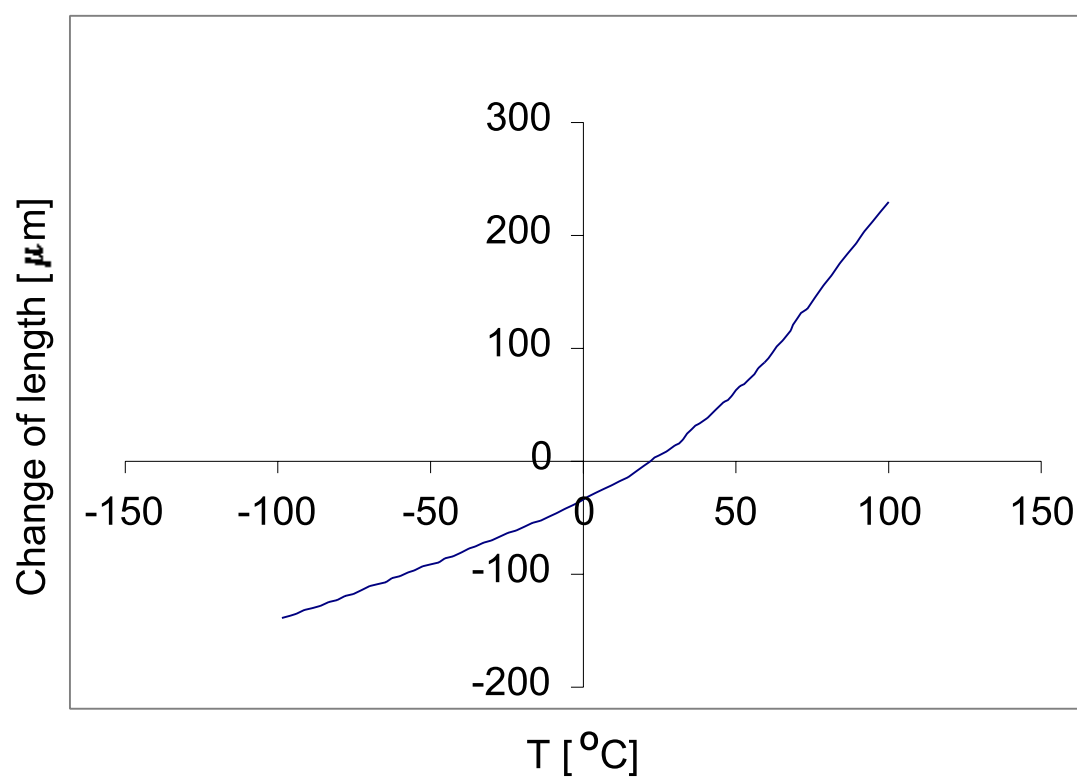


Figure 4.11: CTE data for Flexolith 216R

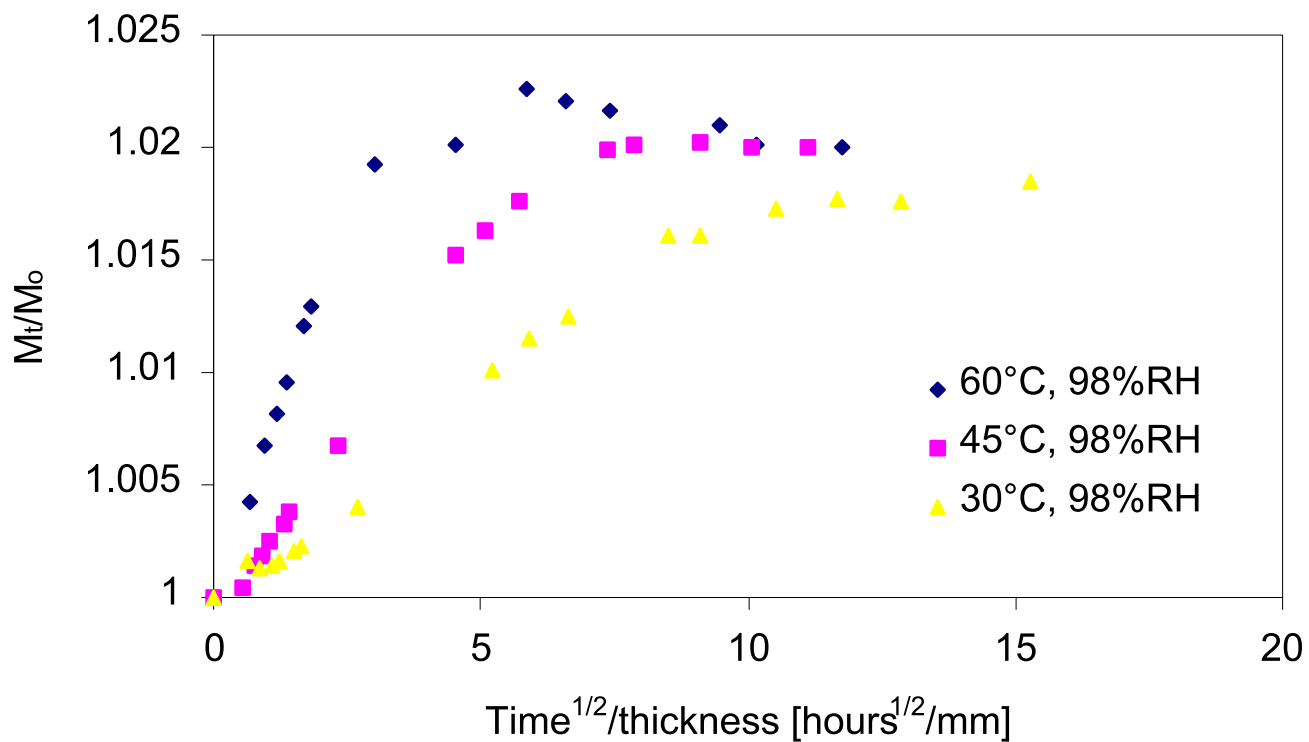


Figure 4.12: Water mass uptake curves for Flexolith 216R under different conditions

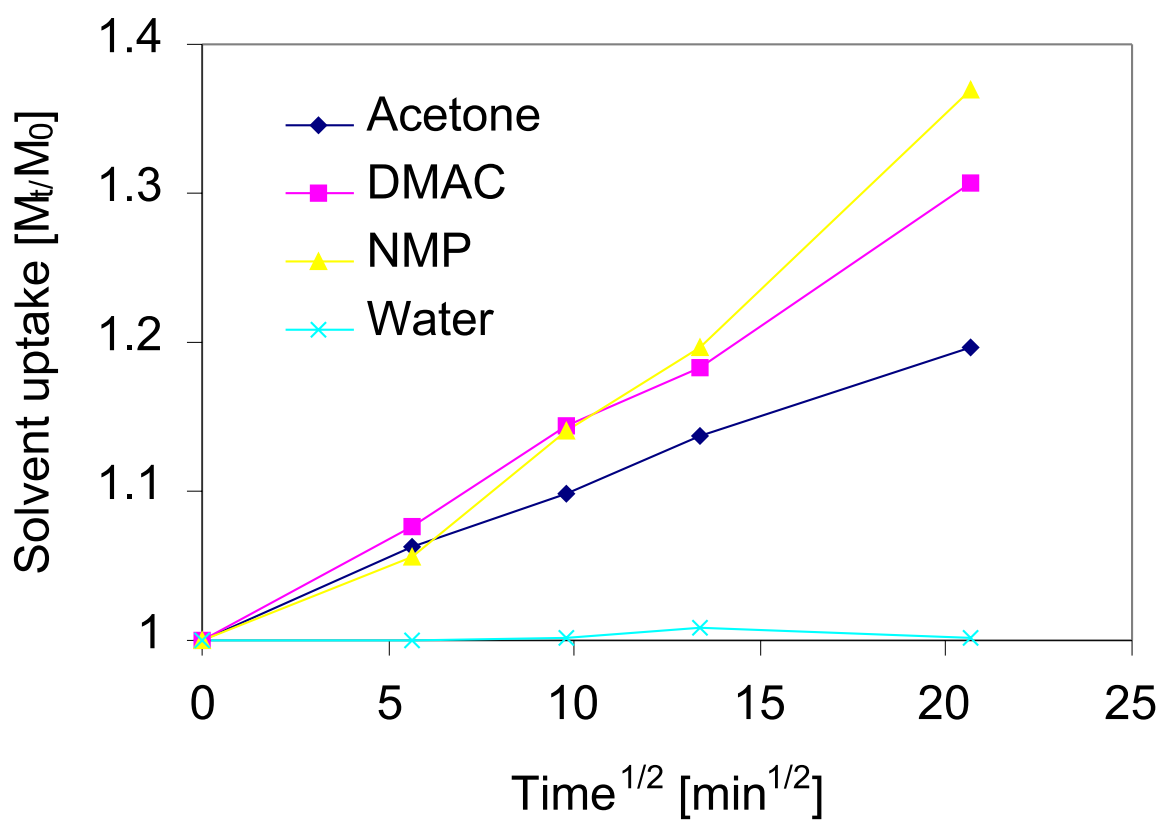


Figure 4.13: Different solvent mass uptake curves for Flexolith 216R

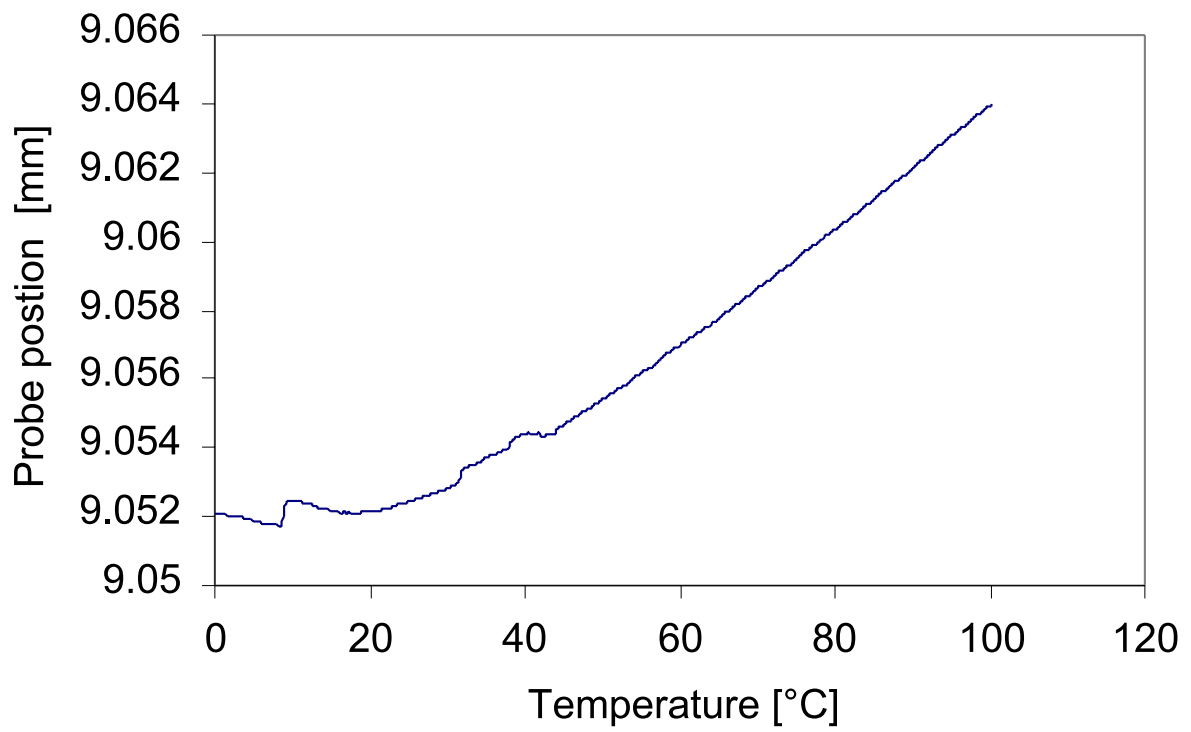


Figure 4.14: CTE data for aluminum

Table 4.1: Tensile test results of PC

Temperature	Crosshead rate	Elastic Modulus	Poisson's ratio
RT	2 mm/min	5.1 <i>GPa</i>	0.21
RT	10 mm/min	6.0 <i>GPa</i>	0.21
-33°C	1 mm/min	9.2 <i>GPa</i>	0.19

Table 4.2: Tensile test results of neat polymer

Temperature	Crosshead rate	Elastic modulus	Poisson's ratio
RT	1 mm/min	1.1 <i>GPa</i>	0.41
RT	10 mm/min	1.7 <i>GPa</i>	0.39
-33°C	1 mm/min	2.8 <i>GPa</i>	0.39

Table 4.3: The properties of Al alloy 6063-T6

Material	Elastic modulus	Yield stress	CTE
Al	68 GPa	227 MPa	$27 \times 10^{-6}/^{\circ}C$

# Chapter 5

## Improving Bonds to Cured Epoxy

### 5.1 Introduction

One polymer concrete bridge has been built in Virginia by Reynolds Metals Company. The bridges are located in the places with small traffic volume, which can be good for a field study. After three months of service, the coating began to debond from the aluminum decks.

After an investigation, the major reason as reported by Reynolds Metals Company was as follows. The bridge decks of aluminum beams coated with polymer concrete (epoxy mixed with a silica sand aggregate) were constructed at the factory. The aluminum bridge decks were bolted together at the construction site, as shown in figure 5.1. At the construction site, fresh polymer concrete was applied between the previously (factory) cured polymer concrete coatings at the Al beam-PC joints (see figure 5.1). It was easier for crack to start at the interface of the new epoxy and old epoxy. Once the crack started, the crack allowed moisture and other undesirable substances such as salt get in to affect the bond between the polymer coating and aluminum. One way to help prevent this potential cause of delamination is to fill the crack with fresh epoxy. The bond between the old cured epoxy and new fresh epoxy is not strong. Still the crack propagated between the epoxy and the aluminum substrate.

One method to solve this real problem is proposed in this study. Dimethylacetamide (DMAC), a powerful organic solvent, was used to promote bonding between fresh and cured epoxy. The samples treated with DMAC are compared with those not treated.

Additionally, this study provided some information about cohesive failure of this material system. Double cantilever beam (DCB) specimens were used to investigate this cohesive failure mode.

## 5.2 Static DCB Testing

### 5.2.1 Introduction

Double cantilever beam testing is a common experimental method for studies concerned with the fracture toughness of adhesive joints. Williams [7] gave the analysis of DCB specimens, and showed that the corrected beam theory is accurate and reliable. Blackman [8] gave the calculation of adhesive fracture energies from DCB test specimens. Rakestraw [9] showed research on the rate dependence of the DCB testing.

### 5.2.2 Testing and analytical solution

Specimens were produced by bonding  $200 \times 24.7 \times 6.35$  mm strips of aluminum (provided by Reynolds Metals Company) with an adhesive thickness of 1 mm, as shown in figure 5.2. The pretreatment of aluminum bars was phosphoric acid, which can provide a very strong bond. A schematic of the symmetric DCB is shown in figure 5.3.

DCB specimens were tested in an Instron 4505 machine controlled through its GPIB interface using LabVIEW<sup>1</sup> software. A crosshead rate of 1 mm/min was used. When the specimen was loaded, the load versus displacement curve was linear. The critical energy

---

<sup>1</sup>LabVIEW is a software developed by National Instruments CO. , TX

release rate  $G_{Ic}$  was obtained when the crack had begun to grow. One typical loading and unloading curve is shown in figure 5.4.

The crack did not propagate in a stable manner. When the load reached the maximum and began to decrease rapidly, the crosshead motion was held to allow crack growth to continue until it approached equilibrium conditions.

The fracture energy for the static DCB test was determined using Eqn 5.1, which was derived from the compliance method Eqn. 5.2 (Irwin and Kies [38]).

$$G = \frac{P^2 a^2}{bEI} = \frac{12P^2 a^2}{b^2 E h^3} \quad (5.1)$$

$$G = \frac{1}{2b} P^2 \frac{\partial C}{\partial a} \quad (5.2)$$

Where,  $P$  is the force at the onset of crack growth,  $a$  the crack length,  $b$  the specimen width,  $C$  the compliance of the test specimen, which can be determined experimentally,  $E$  the modulus of the adherend, and  $h$  the thickness of the adherend.

### 5.2.3 Testing results and analysis

Since only two or three load cycles can be conducted on each specimen, it was not possible to use the compliance method 5.2 to do data analysis, which was more accurate. During the experiments, the initial crack length  $a$  was read and the critical load value  $P$  was calculated. Eqn 5.1, the strain energy release rate  $G$  was obtained. The qualitative energy release rate values of for three kinds of DCB specimens (see figure 5.1) are shown in table 5.1.

One specimen with DMAC had a much higher  $G$  value than the other two specimens without DMAC. Another specimen with DMAC had a similar  $G$  value to the other two specimens without DMAC. For the second cycle, both of the specimens with DMAC had higher  $G$  values than the specimens without DMAC. For the third cycle, the specimen with DMAC had a higher  $G$  value than the two specimens without DMAC. Other important

information obtained was that the G value of the specimens with DMAC had a similar G value to the specimens with fresh epoxy layer inside, which indicated that they had the same failure mode - cohesive failure. Although the data had some scatter, it is concluded that the samples with DMAC treatment can provide a better bond.

Moreover, important information was obtained by examining the failed fracture surface. For the sample without DMAC, the failure occurred at the bond between the fresh and cured epoxy, see figure 5.5. For the specimens with DMAC, the wave-like pattern revealed that the crack occurred in the adhesive but not at the bond between the fresh and cured epoxy, see figure 5.6. The finding also showed that DMAC on cured epoxy helped form a better bond.

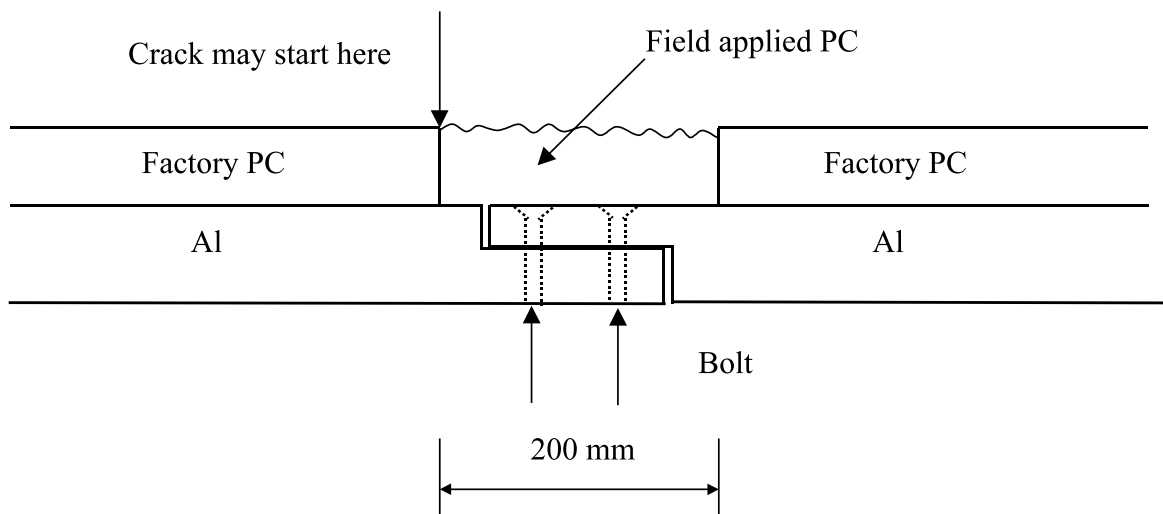


Figure 5.1: Schematic of a filled joint

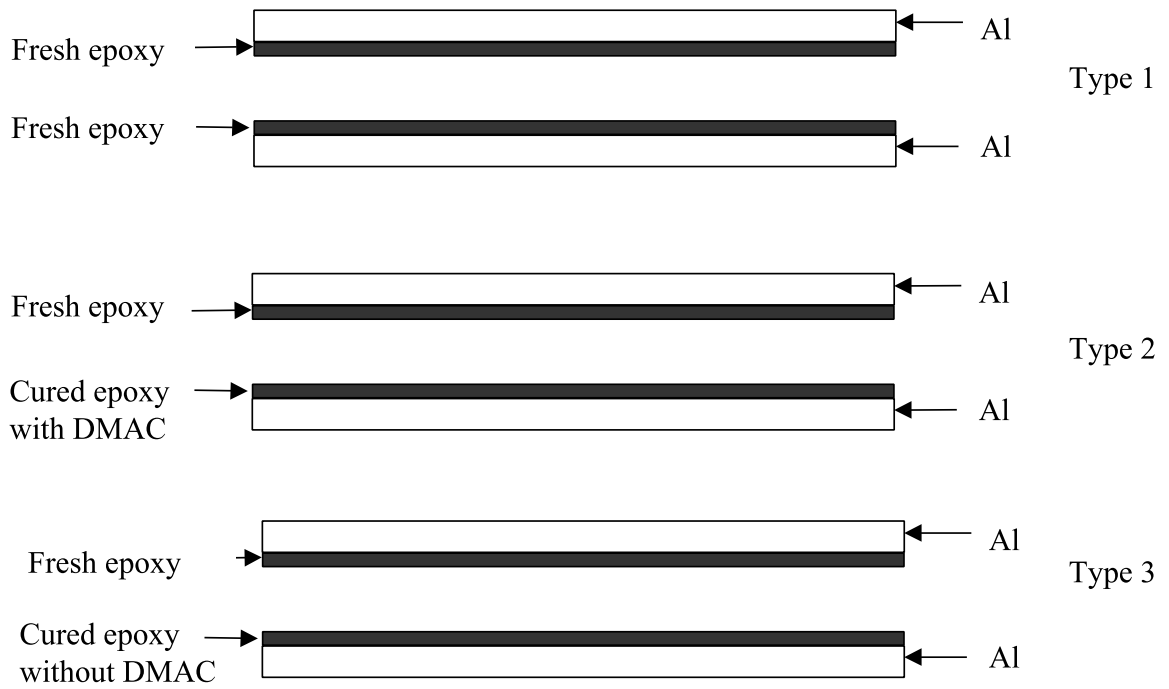


Figure 5.2: Three types of DCB specimens

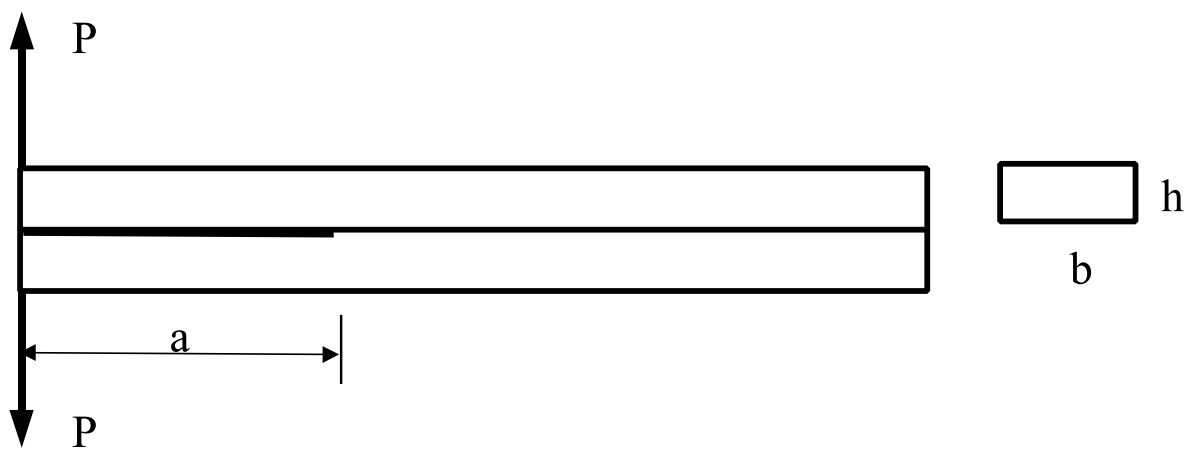


Figure 5.3: Schematic of symmetric DCB, pure mode I

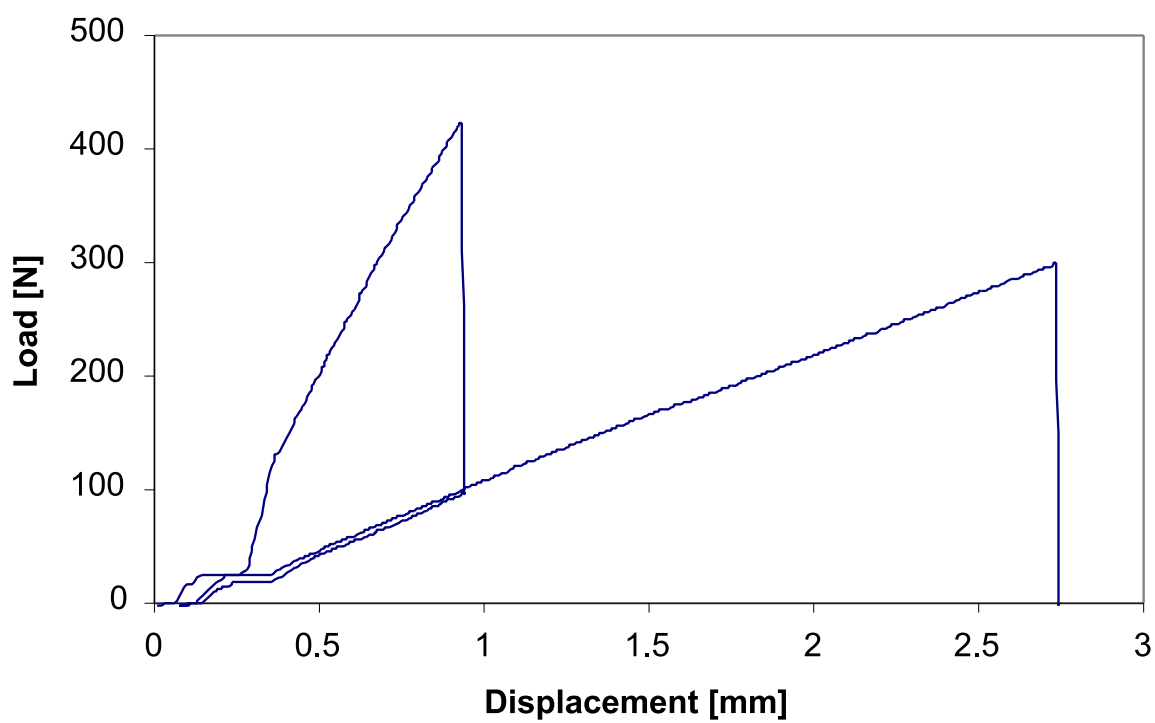


Figure 5.4: Load and unload curve for DCB testing

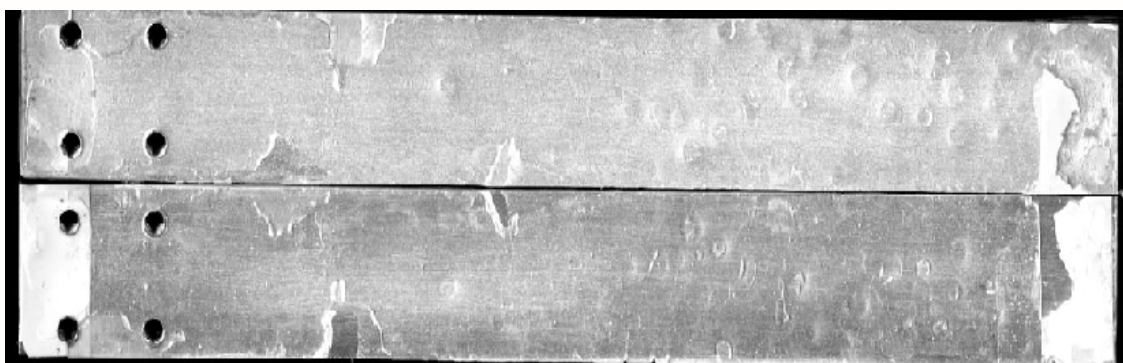


Figure 5.5: Photograph of the failure surface of a DCB specimen without DMAC

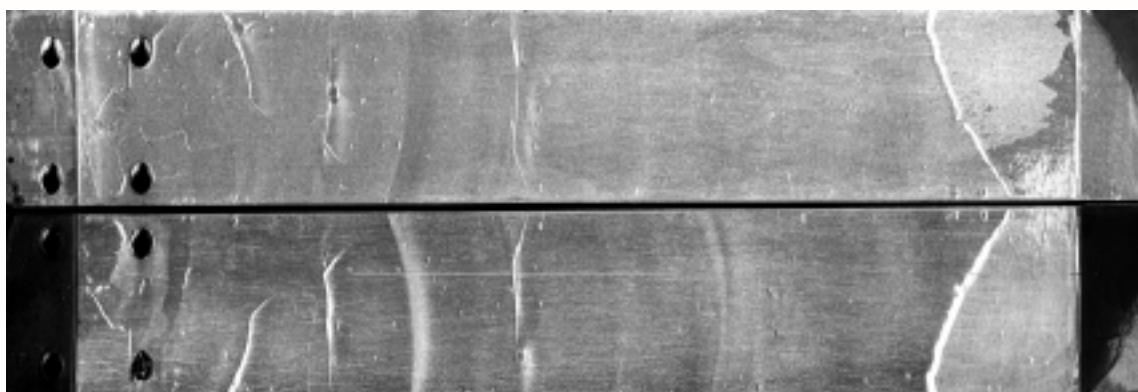


Figure 5.6: Photograph of the failure surface of a DCB specimen with DMAC

Table 5.1: DCB test results for G

$G_{max}$	Fresh epoxy	DMAC #1	DMAC #2	No DMAC #1	No DMAC #2
1 <sub>st</sub> cycle	300.3	434	184	89.3	204
2 <sub>nd</sub> cycle	433	402	224	152.4	188
3 <sub>rd</sub> cycle			227	95.4	127

# Chapter 6

## Conclusions

Polymer concrete coated aluminum bridge decks are built for the purpose of solving the problem of chloride-induced corrosion of steel-reinforced concrete bridge decks. The performance of the bridge systems under a variety of environments needs to be investigated. This research study evaluated the durability of the polymer concrete coating on the aluminum bridge decks.

This research has developed a modified mix-mode fracture (MMF) test method which can be used to measure the fracture toughness of the bond between polymer concrete and aluminum bridge decks. Plastic deformation of the aluminum substrate is avoided using the modified MMF test. Each sample can be tested twice and only one debond tip propagates each time, thus simplifying the monitoring of debond growth. The cure of an adhered layer on a substrate may result in shrinkage and corresponding residual tensile stress. A sandwich fashioned specimen can make the residual stresses less important.

The MMF method was effective for evaluating the durability of polymer concrete bonds to aluminum bridge decks. The downward trends in the critical strain energy release rate showed that the fracture toughness decreased with increasing aging time. However, for some specimens aged at 60°C with/without humidity, the epoxy/aggregate bond was degraded over time, which resulted in crack extension within the coating. Bond fracture toughness

could not be determined for the specimens because failure occurred within the coatings.

Both visual and SEM showed that the failure locus of the MMF specimens was close to the interface. Only a small amount of epoxy was left on the aluminum substrate. For those specimens aged at 60°C with/without humidity, adhesive failure within the coating was observed, and the coating tended to have a higher level of degradation than the PC/Al bond.

A finite element model was constructed for the sandwich specimen. The numerical analysis provides J-integral values, which are in reasonable agreement with  $G$  calculated from the analytical solution. The numerical analysis gave a solution which is higher than the results from analytical solution. One possible reason is that the analytical evaluation used a simple beam theory. The dimensions of the specimen have a length to depth ratio of 7 and a length to width ratio of 4. The specimen we used is not a perfect for simple beam theory. In this case, the finite element analysis should give more accurate solution than analytical evaluation.

During the research, some problems were encountered. Although the viscoelastic property of the adhesive was good for stress relief, it resulted in difficulties when carrying out fracture tests. The polymer concrete coating showed extensive time-dependence of elastic modulus at room temperature. Viscoelastic flow in the polymer concrete reduced the available strain energy release rate. The results of relaxation tests at room temperature and at -33°C showed that decreasing the test temperature can reduce the influence of the viscoelasticity. The test technique included conditioning the specimens in dry ice for 5 hours before testing. The testing temperature was assumed to be -33°C, the temperature of dry ice. The aluminum substrate and coating are thick, so specimens with large dimensions had to be chosen. Unfortunately, the dimensions of the specimens were limited by the conditioning chambers and testing frame. The final dimensions of the specimens were not perfect for

beam theory analysis. The PC is an inhomogeneous material because it consisted of a high volume and irregularly shaped of aggregate. The coating has many voids and defects inside, which may contribute to the scatter of the fracture test data. Aging affected the polymer concrete coating (silica aggregate /epoxy bond), so it was not possible to obtain the fracture toughness of the bond between PC and the aluminum substrate for several conditions after six to twelve months of aging.

The studies helped to understand the adhesive bonds and how they were affected by environment factors. The information could help to predict the service life of the polymer concrete aluminum bridge systems.

The author suggests some future research work on the epoxy/aggregate bond. This bond may cause problem during bridge's service life before the polymer concrete coating debonds from the aluminum bridge deck.

# Bibliography

- [1] M. M. Sprinkel, R. Sellers, and R. E. Weyers. Concrete bridge protection and rehabilitation: Chemical and physical technique, rapid concrete bridge deck protection, repair and rehabilitation. *National Research Council*, SHRP-S-344, 1993.
- [2] D. G. Walters and B. F. Schafran. Guide for polymer concrete overlays. *ACI*, (548.5R-94):2–3, January 1994.
- [3] J. J. Ahlskog. Aluminum bridge decks - a viable economic alternative. *International Bridge Engineers Conference*, IBC-96-12, 1996.
- [4] D. W. Garber and B. Robbins. Evaluation of polymer concrete wearing surface for aluminum bridge decks. *Transportation Research Board, mtg*, 1997.
- [5] A. J. Kinloch. *Adhesion and Adhesive-Science and Technology*. Chapman and Hall, London, 1987.
- [6] S. Mostovoy and E. J. Ripling. *J. of Appl. Poly. Sci.*, 10:1351–1371, 1966.
- [7] S. Hashemi, A. J. Kinloch, and J. G. Williams. The analysis of interlaminar fracture in uniaxial fibre-polymer composites. *Proc. R. Lond.*, A(427):173–199, April 1989.
- [8] B. Blackman, J. P. Dear, A. J. Kinloch, and S. Osiyemi. The calculation of adhesive fracture energies from double-cantilever beam test specimens. *J. of Mate. Sci. Lett.*, 10:253–256, 1991.

- [9] M. D. Rakestraw, M. W. Taylor, and D. A. Dillard. Time dependent crack growth and loading rate effects on interfacial and cohesive fracture of adhesive joints. *J. Adhesion*, 55:123–149, 1995.
- [10] S. Mall and W. S. Johnson. Characterization of mode I and mixed-mode failure of adhesive bonds between composite adherends. *Composite Materials: Testing and Design*, ASTM STP 893:322–334, 1986.
- [11] B. R. K. Blackman, J. P. Dear, A. J. Kinloch, H. Macgillivray, Y. Wang, J. G. Williams, and P. Yayla. The failure of fibre composites and adhesively bonded fibre composites under high rates of test. *J. Mater. Sci*, 30:5885–5900, 1995.
- [12] A. J. Russell and K. N. Street. Moisture and temperature effects on the mix-mode delamination fracture of unidirectional graphite/epoxy. *Delamination and Debonding of Materials*, (ASTM STP 876):349–370, 1985.
- [13] B. D. Davidson and V. Sundararaman. A single leg bending test for interfacial fracture toughness determination. *Int. J. Fracture*, 78:193–210, 1996.
- [14] J. E. Ritter, T. J. Lardner, A. J. Stewart, and G. C. Prakash. Crack propagation in polymer adhesive/glass sandwich specimens. *J. Adhesion*, 49:97–112, 1995.
- [15] J. E. Ritter, T. J. Lardner, W. Grayeskl, G. C. Parkash, and J. Lawrence. Fatigue crack propagation at polymer adhesive interface. *J. Adhesion*, 63:265–284, 1997.
- [16] P. G. Charalambides, J. Lund, A. G. Evans, and R. M. McMeeking. A test specimen for determining the fracture resistance of bimaterial interfaces. *J. Applied Mechanics*, 56:78–82, March 1989.
- [17] N. W. Klingbeil and J. L. Beuth. Interfacial fracture testing of deposited metal layers under four-point bending. *Engineering Fracture Mechanics*, 56(1):113–126, 1997.
- [18] Z. Zhang and J. K. Shang. Subcritical crack growth at bimaterial interfaces: Part 1. flexural peel technique. *Metallurgical and Materials Transactions A*, 27A:205–211, 1996.

- [19] H. C. Cao and A. G. Evans. An experimental study of the fracture resistance of bimaterial interfaces. *Mechanics of Materials*, 7:295–304, 1989.
- [20] T. Chang, E. A. Sproat, Y. H. Lai, N. E. Shephard, and D. A. Dillard. A test method for accelerated humidity conditioning and estimation of adhesive bond durability. *J. Adhesion*, 60:153–162, 1997.
- [21] M. D. Chang, K. L. Devries, and M. L. Williams. The effects of plasticity in adhesive fracture. *J. Adhesion*, 4:221–231, 1972.
- [22] A. J. Kinloch and R. J. Young. *Fracture Behavior of Polymers*. Applied Science Publishers LTD, London, 1983.
- [23] N. W. Klingbeil and J. L. Beuth. Interfacial fracture testing of deposited metal layers under four-point bending. *Engineering Fracture Mechanics*, 56:113–126, 1996.
- [24] F. P. Beer and E. R. Johnston. *Mechanics of Materials*. McGraw-Hill, Inc., Newyork, 2nd edition, 1992.
- [25] P. A. Fay and A. Maddison. Durability of adhesively bonded steel under salt spray and hydrothermal stress conditons. *Int. J. Adhesion and Adhesive*, 10:179–186, 1990.
- [26] L. E. Neilsen and R. F. Landel. *Mechanical Properties of Polymers and Composites*. Marcel Dekker, Inc., New York, 2 edition, 1990.
- [27] A. J. Kinloch. *Durability of Structural Adhesives*. Applied Science Publishers, London, 1983.
- [28] H. Parvatareddy. *Durability of Polymer Adhesives and Their Bonded Joints for High Temperature Application*. Ph.D dissertation, Virginia Polytechnic Institute and State University, <http://scholar.lib.vt.edu/theses/available/etd-111297-125413/>, Blacksburg, VA, 1997.

- [29] M. R. Bowditch. The durability of adhesive joints in the presence of water. *Int. J. Adhesion and Adhesive*, 16:73–79, 1996.
- [30] B. M. Brewis, J. Comyn, A. K. Raval, and A. J. Kinloch. The effect of humidity on the durability of aluminum-epoxide joints. *Int. J. Adhesion and Adhesive*, 10:247–252, 1990.
- [31] B. D. Neve and M. E. R. Shanahan. Effects of humidity on a epoxy adhesive. *Int. J. Adhesion and Adhesive*, 12:191–196, 1992.
- [32] B. M. Parker. Environmental durability of aluminum joints with different pretreatment. *Int. J. Adhesion and Adhesive*, 13:47–51, 1993.
- [33] J. W. Holubka, W. Chun, and R. A. Dickie. Durability of adhesive bonds to zinc-coated steels: Effects of corrosive environments on lap shear strength. *J. Adhesion*, 30:173–183, 1989.
- [34] R. D. Adams, J. Coppedale, V. Mallick, and H. Al-Hamdan. The effect of temperature on the strength of adhesive joints. *Int. J. Adhesion and Adhesive*, 12:185–190, 1992.
- [35] D. R. Arnott and M. R. Kindermann. Durability testing of epoxy adhesive bonds. *J. Adhesion*, 48:101–119, 1995.
- [36] H. F. Brinson. *Engineered Materials Handbooks: Adhesive and Sealants*, volume V3. ASM International, USA, 1990.
- [37] S. L. Rosen. *Fundamental Principles of Polymeric Materials*. Weley, New York, 1993.
- [38] G. R. Irwin and A. Kies. *Journal of Welding*, 33:193, 1954.
- [39] E. Moussiaux. *Bending of a bonded beam as a test method for adhesive properties*. MS thesis, Virginia Polytechnic Institute and State University, Blacksburg, VA, 1987.
- [40] J. Whitney and R. McCullough. *Micromechanical Materials Modeling*. Technomic Publishing Company, Inc., Pennsylvania, USA, 1990.

- [41] Z. Hashin. The elastic moduli of heterogeneous materials. *J. Applied Mechanics*, (61-WA-39):1–8, 1960.
- [42] B. Wunderlich. *Thermal Analysis*. Academic Press, Boston, 1990.
- [43] J. M. G. Cowie. *Polymers: Chemistry and Physics of Modern Materials*. Blackie Academic and Professional, UK, 2 edition, 1991.
- [44] R. A. Gledhill, A. J. Kinloch, and S. J. Shaw. A model for predicting joint durability. *Journal of Adhesion*, 11:3–15, 1980.

# Appendix A

## ABAQUS Input File - Sandwich Specimen

This ABAQUS program can investigate the J-intergral and the stresses.

\*HEADING

J-INTERGRAL FOR BRIDGE

\*NODE

\*\*RIGHT SIDE OF CRACK (NODE LISTED BOTTOM TO TOP)

4057,0.01,-0.011

4065,0.01,0.0

4001,0.01,0.0

4009,0.01,0.008

804009,0.01,0.0173

\*\*LEFT ENDPOINT OF CRACK

1, 0.0, 0.0

65, 0.0, 0.0

\*\*LEFT SIDE OF THE CRACK (NODES LISTED BOTTOM TO TOP)

4041,-0.01,-0.011

4033,-0.01, 0.0

```
4025,-0.01,0.008
804025, -0.01,0.0173
**LEFT VERTICAL BOUNDARY
20041, -0.1093,-0.011
20033, -0.1093, 0.0
20025, -0.1093, 0.008
820025, -0.1093, 0.0173
**RIGHT VERTICAL BOUNDARY
8057,0.0307, -0.011
8065, 0.0307, 0.0
8001, 0.0307, 0.0
8009, 0.0307, 0.008
808009, 0.0307, 0.0173
**MOST RIGH
28057, 0.1807,-0.011
28065, 0.1807, 0.0
28073, 0.1807, 0.008
28081, 0.1807, 0.0173
**NEW NODE
8073,0.0307, 0.008
8081,0.0307, 0.0173
*NGEN, NSET=TIP
1,65
*NGEN,NSET=OUTER
4001, 4009
4009, 4025
4025,4033
4033,4041
```

4041,4057  
4057,4065  
\*NFILL, SINGULAR=1  
TIP, OUTER, 40, 100  
\*NGEN, NSET=RIGHT2  
8057,8065,1  
\*NGEN  
8065,8073,1  
\*NGEN  
8073,8081,1  
\*NGEN  
28057, 28081,1  
\*NGEN, NSET=INTER4  
4009, 4025,1  
\*NGEN, NSET=INTER3  
4025, 20025,100  
\*NGEN, NSET=UP2  
804009, 804025,1  
\*NGEN, NSET=UP1  
804025,820025,100  
\*NGEN, NSET=UP3  
804009, 808009,100  
\*NGEN,NSET=INTER5  
4009,8009,100  
\*NGEN, NSET=UP4  
4001,8001,100  
\*NGEN, NSET=DOWN4  
4065,8065,100

```
*NGEN,NSET=DOWN3
4057,8057,100
*NGEN,NSET=DOWN1
4041, 20041, 100
*NGEN, NSET=INTER1
4033, 20033,100
*NGEN, NSET=NEW1
8057, 28057, 100
*NGEN, NSET=NEW2
8065, 28065, 100
*NGEN, NSET=NEW3
8073, 28073, 100
*NGEN, NSET=NEW4
8081, 28081, 100
*NFILL
INTER4,UP2, 8, 100000
INTER3,UP1, 8, 100000
DOWN3, DOWN4, 8,1
UP4, INTER5, 8,1
INTER5, UP3, 8, 100000
INTER3, INTER1, 8, 1
INTER1, DOWN1,8,1
NEW1, NEW2, 8,1
NEW2, NEW3, 8, 1
NEW3, NEW4, 8, 1
*ELEMENT,TYPE=CPS8
1,1,201,203,3,101,202,103,2
641,4025,4225,4227,4027,4125,4226,4127,4026
```

1281,4057,4257,4259,4059,4157,4258,4159,4058  
1361,4001,4201,4203,4003,4101,4202,4103,4002  
1441,4009,4209,204209,204009,4109,104209,204109,104009  
1521,4011,4009,204009,204011,4010,104009,204010,104011  
1553,4225,4025,204025,204225,4125,104025,204125,104225  
1873, 8057, 8257, 8259, 8059, 8157, 8258, 8159, 8058  
2273, 8065,8265,8267,8067,8165,8266,8167,8066  
2673, 8073,8273,8275,8075,8173,8274,8175,8074

\*ELGEN

1,20,200,1,32,2,20  
641,80,200,1,8,2,80  
1281,20,200,1,4,2,20  
1361,20,200,1,4,2,20  
1441,20,200,1,4,200000,20  
1521,8,2,1,4,200000,8  
1553,80,200,1,4,200000,80  
1873,100,200,1,4,2,100  
2273,100,200,1,4,2,100  
2673,100,200,1,4,2,100

\*ELSET,ELSET=ADHES,GENERATE

1,320  
641,960  
1361,1440  
2273,2672

\*ELSET,ELSET=ADHER,GENERATE

321,640  
961,1360  
1441,2272

```
2673,3072
*MATERIAL,NAME=AL
*ELASTIC
68.E9,0.33
*MATERIAL,NAME=EPOXY
*ELASTIC
9.2E9, 0.21
*SOLID SECTION,ELSET=ADHES,MATERIAL=EPOXY
0.051
*SOLID SECTION,ELSET=ADHER,MATERIAL=AL
0.051
*BOUNDARY
820025,2,2
15381,2,2
*STEP,INC=1000,NLGEOM
*STATIC
*CLOAD
12341,2,2605
*CONTOUR INTEGRAL,FREQUENCY=1000,CONTOURS=19,OUTPUT=BOTH
TIP,-1.,0.
*EL PRINT,FREQUENCY=1000
S
*NODE PRINT,FREQUENCY=1000
U
*RESTART,WRITE
*END STEP
```

## Vita of Huiying Zhang

Huiying Zhang, daughter of Xinyi Zhang and Shuqing Chen, was born on November 7, 1972. Upon graduating from high school in Shenyang, a big industrial city in northern China, she attended Beijing University of Aeronautics and Astronautics majoring in aircraft design and engineering mechanics. After obtaining her Bachelors degree in 1995, she enrolled in the graduate school of the same university. In August 1996, she transferred to Virginia Polytechnic Institute and State University in Blacksburg (US) and worked for her masters degree in engineering science and mechanics under Dr. David A. Dillard. Upon her graduation, she hopes to find a job doing research related to her major.